Sensitivity of pelagic calcification to ocean acidification

R. Gangstø[1, 2, *], F. Joos[1, 3] and M. Gehlen[2]

[1] {Climate and Environmental Physics, Physics Institute, University of Bern, Sidlerstrasse 5, 3012 Bern, Switzerland}

[2] {LSCE/IPSL, Laboratoire des Sciences du Climat et de l'Environnement, CEA-CNRS-UVSQ, Orme des Merisiers, Bât. 712, CEA/Saclay, 91198 Gif-sur-Yvette Cedex, France}

[3] {Oeschger Centre for Climate Change Research, University of Bern, Zähringerstr. 25, 3012 Bern, Switzerland}

[*] {now at: Federal Office of Meteorology and Climatology, MeteoSwiss, Zurich, Switzerland}

Correspondence to: R. Gangstø (reidun.gangsto@meteoswiss.ch)

Abstract

Ocean acidification might reduce the ability of calcifying plankton to produce and maintain their shells of calcite, or of aragonite, the more soluble form of $CaCO_3$. In addition to possibly large biological impacts, reduced $CaCO_3$ production corresponds to a negative feedback on atmospheric CO_2. In order to explore the sensitivity of the ocean carbon cycle to increasing concentrations of atmospheric CO_2, we use the new biogeochemical Bern3D/PISCES model. The model reproduces the large scale distributions of biogeochemical tracers. With a range of sensitivity studies, we explore the effect of i) using different parameterizations of $CaCO_3$ production fitted to available laboratory and field experiments, of ii) letting calcite and aragonite be produced by auto- and heterotrophic plankton groups, and of iii) using carbon emissions from the range of the most recent IPCC Representative Concentration Pathways (RCP). Under a high-emission scenario, the $CaCO_3$ production of all the model versions decreases from ~1 Pg C yr^{-1} to between 0.36 and 0.82 Pg C yr^{-1} by the year 2100. The changes in $CaCO_3$ production and dissolution resulting from ocean acidification provide only a small feedback on atmospheric CO_2 of 1-11 ppm by the year 2100, despite the wide range of parameterizations, model versions and scenarios included in our study. A potential upper limit of the CO_2-calcification/dissolution feedback of -30 ppm by the year 2100 is computed by setting calcification to zero after 2000 in a high 21s century emission scenario. The similarity of feedback estimates yielded by the model version with calcite produced by nanophytoplankton and the one with calcite, respectively aragonite produced by mesozooplankton suggests that, at present, expending biogeochemical models to calcifying zooplankton might not be needed to simulate biogeochemical impacts on the marine carbonate cycle. The changes in saturation state confirm previous studies indicating that future anthropogenic CO_2 emissions may lead to irreversible changes in Ω_A for several centuries. Furthermore, due to the long-term changes in the deep ocean, the ratio of open water $CaCO_3$ dissolution to production stabilizes by the year 2500 at a value that is 30-50% higher than at pre-industrial times when carbon emissions are set to zero after 2100.

1 Introduction

Ocean uptake of atmospheric CO_2 leads to a decrease in carbonate ion concentrations, a reduction in pH, a shoaling of the calcium carbonate ($CaCO_3$) saturation horizons, and a subsequent increase in $CaCO_3$ dissolution. The current rate at which this process, known as ocean acidification, is occurring will likely have large biological consequences for ocean

ecosystems within the near future. Past studies reported a decrease in calcification with decreasing saturation state before undersaturation is reached (refer to Fabry et al. (2008) for a synthesis of existing experimental evidence). Calcifying plankton (mainly coccolithophores, foraminiferas, and pteropods (Schiebel, 2002; Kleypas et al., 2006)) might be especially vulnerable to the decreasing saturation state as these organisms secrete calcite and aragonite, two important forms of $CaCO_3$, to form their shells. In addition to potentially large impacts on the marine calcifiers, a decrease in $CaCO_3$ production causes a higher ocean uptake of CO_2, i.e. a negative feedback on atmospheric CO_2.

The goal of this study is to document the performance of a new cost-efficient 3-dimensional circulation-marine ecosystem model and to apply this Bern3D/PISCES model to study calcification under ocean acidification and related feedbacks to atmospheric CO_2. We address uncertainties by applying a wide range of parameterizations for the dependency of calcification on the chemical state of surface water and for a range of 21st century and long-term CO_2 emission scenarios. A novel parameterization for the production of calcite by zooplankton is introduced and its impact on the cycle of $CaCO_3$ and on atmospheric CO_2 is evaluated. The combination of a cost-efficient circulation model and a complex marine ecosystem model allows us to go a step beyond existing studies in terms of tested parameterizations and scenarios. It is, as far as we are aware of, the first time that calcite production by mesozooplankton is considered in global change simulations.

The following chain of feedbacks in considered in this model study. Anthropogenic emissions cause atmospheric CO_2 to rise, carbon uptake by the ocean to increase, and carbonate ion concentration and the saturation state with respect to $CaCO_3$ to decrease. In response, production and dissolution of $CaCO_3$ change and affect the concentration of dissolved inorganic carbon (DIC) and alkalinity, and in turn, the CO_2 partial pressure in surface water and CO_2 uptake by the ocean. Finally, the altered ocean uptake leads to a different evolution of atmospheric CO_2 as compared to a situation where the $CaCO_3$ cycle would not respond to changes in CO_2 and the saturation state. The production of $CaCO_3$ removes DIC, but twice as much alkalinity from the water; the combined effect of removing DIC and alkalinity is to increase pCO_2 (Frankignoulle et al., 1994). Thus, a decrease in $CaCO_3$ production and the related increase in DIC and alkalinity, tends to increase carbon uptake and to lower atmospheric CO_2. Similarly, shallower dissolution of $CaCO_3$ tends to increase DIC, alkalinity in surface water and to lower pCO_2 in surface waters and in the atmosphere.

Various model experiments have been performed during the recent years in order to identify future changes in calcification rates and associated feedbacks on atmospheric CO_2 (Heinze et al., 2004; Ridgwell et al., 2007, 2009; Gehlen et al., 2007; Hofmann and Schnellnhuber, 2009). The corresponding global biogeochemical models deal with carbonate production as a biogeochemical function rather than attempting to reproduce the complexity of biological responses. Until now, parameterizations of the response of calcification to ocean acidification were generally fitted to experiments done on coccolithophores (mainly *E. huxleyi*) and $CaCO_3$ was on the form of calcite only. With the exception of the study by Ridgwell et al. (2007), which provided a relatively large CO_2 - $CaCO_3$ production/dissolution feedback response to atmospheric CO_2 when simulating continued carbon emissions after the year 2100, all model experiments projected a small CO_2 - $CaCO_3$ feedback on atmospheric CO_2. Ridgwell et al. (2007) estimated that the response of *E. huxleyi* to increasing atmospheric CO_2 is quite small compared to other coccolithophore species, foraminifera and corals. It is thus possible that biogeochemical models that only let $CaCO_3$ production be associated to *E. huxleyi*, may underestimate the CO_2 - $CaCO_3$ feedback on atmospheric CO_2.

Gangstø et al. (2008) extended the study by Gehlen et al. (2007) to include aragonite and, due to limited data on aragonite producing pteropods, they used a dependency equivalent to Gehlen et al. (2007) to project the response of calcite and aragonite production and dissolution to increasing atmospheric CO_2 concentrations. However, CO_2 - $CaCO_3$ production/dissolution feedbacks were not calculated for this model version. No model has so far explicitly included calcite production by mesozooplanton (foraminifera) and simulated its response to ocean acidification. The sensitivity of the later and associated feedbacks to atmospheric CO_2 to including $CaCO_3$ production by heterotrophs in a biogeochemical model, as well as to the choice of functional relationship between $CaCO_3$ production and seawater chemistry remains an open question.

We are lead to the following questions: How important is the choice of shape of the relationship fitting the response of calcification to changing carbonate chemistry? Would the inclusion of aragonite and calcite produced by zooplankton change the predicted evolution of $CaCO_3$ production and dissolution, as well as the feedbacks on atmospheric CO_2? How fast is the expected reversibility of the ocean chemistry after a CO_2 perturbation? Would this be affected by the future changes in $CaCO_3$ production and dissolution?

The amount of data published about the response of calcifying organisms to increasing CO_2 has augmented over the last few years. Concerning open ocean calcifying organisms,

coccolithophores (and especially *Emiliana huxleyi)* have got much attention (Riebesell et al., 2000; Zondervan et al., 2001, 2002; Sciandra et al., 2003; Delille et al., 2005; Langer et al., 2006; Iglesias-Rodriguez et al., 2008; Shi et al., 2009; Casareto et al., 2009; Godoi et al., 2009; Gao et al., 2009; Müller et al., 2010). However, the number of experiments performed on foraminifera and pteropods is also growing (e.g. Wolf-Gladrow et al., 1999; Bijma et al., 1999; Fabry et al., 2008; Comeau et al., 2009). Despite the continuously increasing number of studies published about the response of plankton to decreasing saturation state there are still large uncertainties related to the future evolution of calcification rates and the associated feedbacks. Due to these uncertainties, a number of sensitivity studies with a model including an advanced representation of the marine ecosystem would be of high advantage. However, these kinds of models typically require large amounts of computing time preventing a cost-efficient evaluation of different parameterizations.

The new Bern3D/PISCES model, a combination of the ecosystem model PISCES and the cost-efficient circulation model Bern3D, allows us to explore the above mentioned questions further. More recent experiments on both coccolithophores (Iglesias-Rodriguez et al., 2008 and Shi et al., 2009) and pteropods (Comeau et al., 2009; J. Büdenbender, S. Lischka and U. Riebesell, personal comm.) permit us to improve previous studies on the response of calcification to increasing levels of atmospheric CO_2. However, due to a still limited quantity of observations available, only "idealized" scenarios may be projected. We have therefore chosen a sensitivity study approach to our work. We split our study into three parts: In the first part we explore the change in calcite production in response to increasing atmospheric CO_2, using different parameterizations of this response. Here, calcite is produced by nanophytoplankton. In the next section we broaden the study to include aragonite and calcite produced by mesozooplankton, investigating changes in production, dissolution and ocean chemistry in addition to quantifying the associated CO_2 – $CaCO_3$ production/dissolution feedbacks. Finally we use a range of emission scenarios to study the sensitivity and evaluate the reversibility of the ocean carbonate system to a CO_2 perturbation.

The formal outline is as follows. In section 2, the Bern3D/PISCES model and the new parameterizations for $CaCO_3$ production are described. Model setup and experiments are described in section 3. Section 4 provides an evaluation of the equilibrium state of the Bern3D/PISCES model with observation-based estimates for circulation and water-mass distribution, $CaCO_3$ production, the distribution of dissolved inorganic carbon and alkalinity and of the saturation state as well as for the global ocean pelagic $CaCO_3$ budget. Section 5

presents the results for transient simulations and projections of atmospheric CO_2, $CaCO_3$ production and dissolution, and of the $CaCO_3$-CO_2 feedback. Concluding remarks follow in section 6.

2 The Bern3D/PISCES model

The Bern3D/PISCES model couples the Bern3D cost-efficient, dynamic ocean circulation model (Müller et al., 2006) and the biogeochemical model PISCES. PISCES was developed within the circulation model NEMO/OPA (Aumont and Bopp, 2006; Gehlen et al., 2006, 2007; Gangstø et al., 2008) which has a relatively high resolution in both time and space requiring large computing resources. The low resolution Bern3D/PISCES model facilitates sensitivity analyses, millennial-scale paleoclimatic studies, and multi-scenario analyses.

2.1 The Bern3D dynamical model

The Bern3D model is a global ocean circulation model (Müller et al., 2006) which is based on the 3-dimensional rigid-lid model of Edwards et al. (1998) and Edwards and Marsh (2005). It has a horizontal resolution of 36 x 36 grid boxes and 32 vertical layers with exponentially increasing thickness towards the ocean bottom. The surface layer has a thickness of 39 meters, the bottom layer of 397 meters. The atmosphere is described by one well mixed box and the formulations of air-sea gas exchange are based on the updated OCMIP-2 protocol (Orr et al. 1999; Najjar and Orr, 1999), and downscaled by 19 % as suggested by Müller et al. (2008). The model is forced with seasonal fields of temperature, salinity and wind stress. Sea surface temperatures and salinities are constrained by using restoring and mixed boundary conditions. Restoring boundary conditions force SST and SSS to remain close to modern-day observational values. With mixed boundary conditions we prescribe freshwater fluxes on the ocean surface instead of SSS, allowing circulation-salinity feedbacks to develop upon perturbation of the model state (Bryan, 1986). An additional freshwater flux correction is applied (by removing freshwater from the Atlantic and distributing it in the North Pacific) in order to intensify and deepen the Atlantic meridional overturning circulation (MOC). The model includes an isopycnal diffusion scheme and Gent-McWilliams parameterization for eddy-induced transport (Griffies, 1998). The standard Bern3D model has been tuned towards data-based chlorofluorocarbon and radiocarbon inventories and is able to capture the large-scale ocean circulation, the characteristics of the most important water masses and the large-scale distributions of a range of ventilation timescale tracers (Müller et al., 2006). The

Bern3D model has been applied for a wide range of studies (e. g. Müller et al., 2008; Sidall et al., 2007; Ritz et al., 2008; Tschumi et al., 2008; Parekh et al., 2008; Gerber et al., 2009, Gerber and Joos, 2010).

In the current study we use the parameter values for the Bern3D model as given by Müller et al. (2006), with a few exceptions. The diapycnal diffusivity has been increased from 1 x 10^{-5} m s^{-2} to 5 x 10^{-5} m s^{-2} and the Atlantic-to-Pacific freshwater flux correction was set equal to 0.2 Sv in order to strengthen the circulation fields and subsequently improve the oxygen and nutrients fields of the biogeochemical model. The time step used for the Bern3D model is reduced by a factor of 2 compared to the standard version (Müller el al., 2006), with the PISCES component called every ~2 hours in order to assure numerical stability. Future atmospheric CO_2 depends also on the evolution of terrestrial carbon sources and sinks, and this is uncertain (e.g. Denman et al. IPCC, 2007). Here, we have not included a land biosphere component as the focus is on the ocean carbonate cycle.

2.2 The PISCES model

PISCES is a global ocean biogeochemical model (Aumont et al., 2003; Aumont and Bopp, 2006; Gehlen et al., 2006) which simulates the biogeochemical cycle of oxygen, carbon and the main nutrients controlling marine biological productivity: nitrate, ammonium, phosphate, silicate and iron. Biological productivity is limited by the external availability of nutrients and light. The model includes two phytoplankton size classes (nanophytoplankton and diatoms) and two zooplankton size classes (microzooplankton and mesozooplankton). The C/N/P ratios are assumed constant for all species. For phytoplankton, the prognostic variables are total biomass, iron, chlorophyll and silicon contents. The internal ratios of Fe/C, Chl/C and Si/C are predicted by the model. For zooplankton, the only prognostic variable is total biomass. The bacterial pool is not modeled explicitly. PISCES comprises three non-living compartments for organic carbon: small particulate organic carbon (POC_s), big particulate organic carbon (POC_b) and semi-labile dissolved organic carbon (DOC). The C/N/P composition of dissolved and particulate matter is also coupled to Redfield stochiometry, whereas the iron, silicon and calcite pools of the particles are fully simulated and their ratios relative to organic carbon are allowed to vary. The particulate detrital pools (POC_s, POC_b, biogenic silica and calcite) are fuelled by mortality, aggregation from nanophytoplankton and diatoms, fecal pellet production and grazing.

The standard version of the model (Aumont and Bopp, 2006) considers $CaCO_3$ in the form of calcite only and assigns calcite production to nanophytoplankton, albeit without dependency of carbonate production on saturation state. The latter was implemented by Gehlen et al. (2007) for the sake of studying the future evolution of the marine carbonate cycle. The version developed for this study distinguishes two mineral phases of $CaCO_3$, aragonite and calcite (Gangstø et al., 2008). Changes in the concentration of $CaCO_3$ in the mineral form *l* arise from production, *Prod*, dissolution with the dissolution rate, λ, and sinking of $CaCO_3$ particles with sinking speed ω:

$$\frac{d}{dt}CaCO_{3,l} = Prod_l - \lambda_l \cdot CaCO_{3,l} - \omega\frac{d}{dz}CaCO_{3,l}\,. \qquad (1)$$

We distinguish between dissolution in the open water and from the ocean bottom. Dissolution in open water occurs only in undersaturated water (Ω<1) and the rate λ is dependent on the saturation state, Ω, with respect to the appropriate mineral phase:

$$\lambda_l = k \cdot (1 - \Omega_l) \qquad \text{for } \Omega_l < 1\,. \qquad (2)$$

$CaCO_3$ particles falling on the ocean floor dissolve immediately in the overlying grid cell independent of Ω. This additional dissolution has only a minor effect on the ocean chemistry. Only the open water dissolution is included in our further calculations and comparisons to observations. Production of $CaCO_3$ assigned to the plankton of type *j* and of mineral phase *l* is taken to be proportional to all the loss terms of this plankton type:

$$Prod_{j,l} = R_{j,l} \cdot \{Loss\ Terms\}_j \quad . \qquad (3)$$

No production of calcite or aragonite occurs if the water is undersaturated with respect to the appropriate mineral phase. In oversaturated water, the fraction $R_{j,l}$ is not allowed to fall below 0.01 or exceed 0.8 (Aumont and Bopp, 2006). The model simulates dissolved inorganic carbon and total alkalinity. The carbon chemistry follows the OCMIP protocol (http://www.ipsl.jussieu.fr/OCMIP). A detailed description of the model including model equations and parameters can be found as auxiliary material in Aumont and Bopp (2006).

In the present study, the model alkalinity field was initialized with a global mean alkalinity value of 2.410 mol m^{-3}, which lies between the global average from GLODAP (Key et al., 2004) and the one from Goyet et al. (2000). In the NEMO/PISCES model, half of the fraction of calcite production that is linked to loss of nanophytoplankton by grazing is assumed to be

dissolved in the guts of zooplankton; only the remaining half affects alkalinity in open water and is added to the $CaCO_3$ pool (Aumont and Bopp, 2006). Here, the percentage of $CaCO_3$ that interacts with the alkalinity pool was increased from 0.5 to 0.85, which slightly improves the alkalinity fields. Nitrogen fixation and denitrification as well as river input and silicate deposition from dust were all set to 0 in the present study. In order to improve low oxygen values at depth and low surface concentrations of nutrients in the Bern3D/PISCES model, resulting from differences in circulation strength between the two dynamical models, the sinking speed of the largest class of particulate organic carbonate (POC_b) was reduced to a constant value of 60 m d^{-1}. Total pre-industrial $CaCO_3$ production is tuned in all setups to about 1.0 Pg C yr^{-1} by adjusting the scaling factors in Equations (4), (9) and (11). The values of the scaling factors are not given as they depend largely on the carbonate chemistry and circulation fields of the model used.

2.2.1 Calcite production by nanophytoplankton

The equations for calcite production by nanophytoplankton in the PISCES model are detailed by Gehlen et al. (2007). The proportion of calcifying phytoplankton is low in oligotrophic regions and calcifiers are often the dominant species when nanophytoplankton blooms. To mimic these conditions, the following parameterization is applied for the fraction of calcite production by nanophytoplankton, $R_{P,C}$ (Aumont and Bopp, 2006):

$$R_{P,C} = f_i \cdot L_{\lim}^{P} \cdot \max\left(0.0001, \frac{T}{2+T}\right) \cdot \max\left(1, \frac{P}{2}\right) \cdot \left(\frac{PIC_C}{POC}\right)_i . \quad (4)$$

In this parameterization, f_i is a scaling factor used to match a global calcite production by nanophytoplankton of about 1.0 Pg C y^{-1} (see Table 1 and 2). L denotes limitation by the availability of phosphate, nitrate, ammonium, and iron and is taken to be identical to the nutrient limitation factor for nanophytoplankton growth. T is water temperature in °C and P is mass of nanophytoplankton, with the term *max(1, P/2)* in units of μmol C l^{-1}. The last factor in above equations denotes the ratio of particulate inorganic (PIC) to organic (POC) carbon for calcifying nanophytoplankton under optimal condition and as a function of the saturation state. In our model parameterization, the global pre-industrial surface ocean has an average PIC_C/POC ratio of about 0.8. Subscript i refers to different parameterizations of PIC_C/POC, and subscript C to calcite.

According to experimental results of the coccolithophore *E. huxleyi* obtained by Riebesell et al. (2000), Zondervan et al. (2001, 2002) and Delille et al. (2005), the calcification rate may

be described by a threshold value of the saturation state below which the calcification decreases rapidly. Gehlen et al. (2007) fitted the PIC_C/POC variable to these experimental results. Since then, new experiments with *E. huxleyi* have been performed (Iglesias-Rodriguez et al., 2008 and Shi et al., 2009). When considering the calcification rates, these studies show an increase with decreasing saturation state, which is in contrast to previous studies on *E. huxleyi*. However, when looking at the PIC-POC values, the data points from these two studies fit well into the group of the other experimental data (Fig. 1a).

Michaelis-Menten type relationship between calcite production and saturation

In previous studies (Gehlen et al., 2007; Gangstø et al., 2008) a Michaelis-Menten approach was adopted for the PIC-POC ratio of calcifying nanophytoplankton, in order to mimic the decreasing calcification with decreasing saturation state (Riebesell et al., 2000; Zondervan et al., 2001; Zondervan et al., 2002; Delille et al., 2005). The PIC-POC ratio for calcifying nanophytoplankton as a function of saturation state is expressed as:

$$\left(\frac{PIC_C}{POC}\right)_{MIC} = \left(\frac{PIC_C}{POC}\right)_{\max} \times \frac{(\Omega_C - 1)}{K_{\max} + (\Omega_C - 1)}, \quad \text{for } (\Omega_C\text{-}1) > 0. \qquad (5)$$

$(PIC_C/POC)_{max}$ is the maximum ratio reached under optimal growth conditions for calcifying organisms, the max value that PIC_C/POC would have on Fig. 1a if the Michalis-Menten curve was extended to $\Omega_C=\infty$. The parameter K_{max} corresponds to a half saturation constant, i. e. the value of $(\Omega_C\text{-}1)$ where PIC/POC equals half the value of $(PIC_C/POC)_{max}$. Finally, Ω_C is the saturation state with respect to calcite.

The values $(PIC_C/POC)_{max}$ and K_{max} were previously set equal to 0.8 and 0.4, respectively (Gehlen et al., 2007; Gangstø et al., 2008). New data published (Iglesias-Rodriguez et al., 2008 and Shi et al., 2009) encourage us to make a new fit, termed MIC1, to the data. Only data without severe light and nutrient limitation are considered (Zondervan et al., 2007), thus excluding one of the data sets from Zondervan et al. (2002), in addition to another data set which should be discarded due to large uncertainties (Zondervan et al., 2002). These two data sets were included in the original fit MIC2. The new fit MIC1 provides an upper limit of the PIC-POC value for calcifying organisms equal to 1.04, whereas K_{max} becomes 1.11. The PIC_C/POC ratio is shifted upwards for high saturation state values for the new fit MIC1 compared to the fit MIC2 (Fig. 1a). We refer to simulations with the new parameterization by the term “CALMIC1”, to those with the original fit by “CALMIC2” (Table 1).

Linear relationships between calcite production and saturation

As the quantity of experiments performed on pelagic plankton is not yet massive, we may question the validity of using a Michaelis-Menten type correlation, and wonder how the use of a linear relationship between $CaCO_3$ production and saturation state would influence projected calcification. No $CaCO_3$ production is allowed in undersaturated water. In parameterization LIN1, (PIC_C/POC) and thus production is forced to go through zero for Ω_C equal 1:

$$\left(\frac{PIC_C}{POC}\right)_{LIN1} = ppcal \cdot (\Omega_C - 1), \quad \text{for } (\Omega_C\text{-}1) > 0, \tag{6}$$

with the slope ppcal equal to 0.19.

In parameterization LIN2, data points are fitted with no forcing (the production is still set to 0 when the saturation state becomes smaller than 1:

$$\left(\frac{PIC_C}{POC}\right)_{LIN2} = ppcal2 + ppcal3 \cdot (\Omega_C - 1), \quad \text{for } (\Omega_C\text{-}1) > 0. \tag{7}$$

The offset ppcal2 is 0.55 and the slope ppcal3 is with 0.06 more than three times smaller than in LIN1 (Fig. 1a). We expect thus a stronger response in calcite production for LIN1 than for the other parameterizations. We refer to the linear parameterization forced through zero (Eq. (6)) by “CALLIN1” and to the unconstrained linear fit (Eq. (7)) by “CALLIN2” (Table 1).

2.2.2 Aragonite production by mesozooplankton

The equations for aragonite production and dissolution are specified in Gangstø et al. (2008). One third of pelagic $CaCO_3$ production is assigned to aragonite producing mesozooplankton as a function of saturation state of seawater with respect to aragonite. This percentage is in the upper range of most estimates. Pelagic aragonite production is reported to contribute ~10% to the total pelagic $CaCO_3$ production by Fabry (1990). However, estimates of aragonite production and fluxes in the pelagic ocean are scarce and cover a large range, extending from 10 to 50% of the total global $CaCO_3$ flux (Berner, 1977; Berger, 1978; Berner and Honjo, 1981; Fabry and Deuser, 1991).

Due to the lack of observations available at the time of this study, the modeled dependency of the calcification on saturation state was done in an equivalent way as for calcite following a Michaelis Menten curve with $(PIC_A/POC)_{max}$ and K_{max} equal to 0.8 and 0.4, respectively. Recently, new data has become available allowing a re-assessment of the parameterization.

Comeau et al. (2009) studied the calcification response of the pteropod *Limacina helicina* to decreasing saturation states and report a decrease in aragonite production of 28% with a reduction in saturation state from 1.9 to 1.0 (CO_2 increased from 350 to 760 μatm). The authors did however not provide the corresponding PIC_A to POC ratios. Another study on *L. helicina* was performed in Kongsfjorden, Spitsbergen, Norway. Here, the PIC_A to POC ratios varied between 0.078 and 0.106 (J. Büdenbender, S. Lischka and U. Riebesell, personal comm.). A linear relationship is developed from the two data sets. We let the maximum PIC_A-POC value from the second study correspond to conditions with Ω_A equal 1.9 and calculate a 28% linear decrease in PIC_A-POC down to Ω_A=1 (Comeau et al. 2009). This results in the parameterization:

$$\left(\frac{PIC_A}{POC}\right)_M = pparag + pparag2 \cdot (\Omega_A - 1), \qquad \text{for } (\Omega_A\text{-}1) > 0, \tag{8}$$

where the offset pparag equals 0.076 and the slope pparag2 is 0.033. The PIC_A-POC ratio is multiplied with mesozooplankton biomass, M, and a scaling factor $f_{M,A}$, which is used to tune the aragonite production to 1/3 of global calcification. The factor $R_{M,A}$ for aragonite production by mesozooplankton becomes:

$$R_{M,A} = f_{M,A} \cdot M \cdot \left(\frac{PIC_A}{POC}\right)_M . \tag{9}$$

In contrast to the factor R, for nanophytoplankton, $R_{M,A}$ does not depend on temperature and nutrient limitation. Following Eq. (3), $R_{M,A}$ is multiplied with the sum of the loss terms for mesozooplankton to yield the aragonite production. We refer to the simulation including the aragonite parameterization (Eq. (9)) and the new Michaelis-Menten parameterization for calcite (Eq. (5)) as "CALARAG" (Table 1).

2.2.3 Calcite production by mesozooplankton

Foraminifers are, in addition to coccolithophores, major calcite producers in the pelagic ocean. They may account for between 32 and 80% of the $CaCO_3$ that accumulates on the sea floor (Schiebel, 2002). They are an important link to the upper trophic levels (e.g. Legendre and Le Févre, 1995; Rowe et al., 2008). Studies of foraminifera show reduced calcification in response to ocean acidification (e.g. Wolf-Gladrow et al., 1999; Bijma et al., 1999; Lombard et al., 2009). Most of these studies include changes in shell weight only. The shell mass was reported to decrease by 4-8% for a doubling of atmospheric CO_2 (Spero et al., 1997; Bijma et al, 1999). Moy et al. (2009) suggest that a decrease in shell weight of 30-35% may have taken

place since pre-industrial times (thus within less than a doubling of atmospheric CO_2). Dissard et al. (2009) confirms the correlation between change in carbonate ions and change in shell weights. Lombard et al. (2009) project a decrease in shell weight of between 20 and 27% within the end of the century. The decrease in shell weight is in some studies reported to be non-linear (Bijma et al., 2002; Kuroyanagi et al., 2009), and in another study linear (Lombard et al., 2009). When it comes to changes in calcification rates of foraminifers, we are only aware of the data by Lombard et al. (2009). They suggest a reduction in calcification rates of between 6 and 13% by the end of this century compared to present day conditions, and these data indicate a linear shape of the response in calcification to increasing atmospheric CO_2.

A linear relationship to simulate the response in calcite production by foraminifera to decreasing saturation state is used here. We have chosen to use the unforced linear dependency on saturation state for the corresponding PIC/POC variable:

$$\left(\frac{PIC_C}{POC}\right)_M = ppcal2 + ppcal3 \cdot (\Omega_C - 1) \qquad \text{for } (\Omega_C\text{-}1) > 0, \tag{10}$$

and to describe the fraction $R_{M,C}$ for calcite production by mesozooplankton:

$$R_{M,C} = f_{M,C} \cdot M \cdot \left(\frac{PIC_C}{POC}\right)_M, \tag{11}$$

where $f_{M,C}$ is again a scaling factor used to tune the calcite production to 1/3 of global calcification. The parameter ppcal2 is set to 0.55 and ppcal3 to 0.06. We refer to the simulation including the aragonite parameterization (Eq. (5)), the new Michaelis-Menten parameterization for calcite (Eq. (1)), and the calcite parameterization from Equations (10) and (11) as “CAL2ARAG”.

2.2.4 Sensitivity of the different parameterizations

To highlight the sensitivity of the parameterizations described in the previous sections, their derivatives d(PIC-POC)/d(Ω) were calculated (Fig. 1b). The derivative of the Michaelis-Menten equations becomes:

$$\frac{d(PIC/POC_C)}{d\Omega_C} = \left(\frac{PIC_C}{POC}\right)_{\max} x \frac{K_{\max}}{(K_{\max} + \Omega_C - 1)^2}. \tag{12}$$

For the linear equations the derivatives correspond to the slope constants 0.1928 (LIN1), 0.0573 (LIN2) and 0.0333 (ARAG).

3 Model setup and simulations

The physical Bern3D model was first integrated over 10,000 years using restoring boundary conditions. Next, air-sea freshwater fluxes were diagnosed and averaged over the last 1,000 years to provide mixed boundary conditions. The model was then switched to mixed boundary conditions, and an additional freshwater flux from the Atlantic to the Pacific was included. The model was further run for 5,000 years. Finally, the PISCES model was added and the Bern3D/PISCES model was integrated over 3,000 years with atmospheric CO_2 concentrations kept constant at 278 parts per million (ppm). All the variables presented in this study (alkalinity, saturation state, $CaCO_3$ production etc) are given as annual means.

Nine model versions are run to explore the projected changes in calcification to increasing atmospheric CO_2 concentrations, six with and three, termed NODEPC, NODEPCA, NODEPC2A, without a dependency of calcification on saturation state (Table 1). Atmospheric CO_2 is prescribed for the period from 1766-2006. From 2007-2100, projected CO_2 emissions of the IPCC scenarios RCP8.5 (referred to as High) and RCP6 (Medium) are used (Van Vuren et al., 2008; Strassmann et al., 2009) in addition to a scenario with zero carbon emissions (Low). Most of the model versions are run with the High scenario only, whereas multi-scenario runs are performed with the CALARAG and NODEPCA versions (Table 1). From year 2100 to year 2500 the CO_2 emissions are set to 0 for the High and Medium scenarios. An additional set of runs is performed with the High scenario and all model versions where the calcification is set to 0 from the year 2000. All scenario runs are accompanied with corresponding control runs with constant pre-industrial CO_2 concentrations.

4 Model evaluation/pre-industrial state

In order to validate the new Bern3d/PISCES model, a thorough model-data comparison is presented next. Pre-industrial model output is compared to pre-industrial observations and observation-based estimates by first removing anthropogenic perturbations from the data sets whenever these were available, such as for DIC and saturation state. For the other variables, we follow common praxis and compare pre-industrial model output with present-day observations, thereby implicitly assuming that the difference between pre-industrial and present-day observations would be small.

4.1 Circulation and water masses

Maximum overturning reaches 23 Sv (1 Sv = 10^6 m^3 s^{-1}) at around 45°N in the North Atlantic, with a southward transport out of the Atlantic between 1,000 and 2,000 m depth of about 16 Sv (Fig. 2). This is comparable to the estimates of Talley et al. (2003) of maximum overturning and southward transport equal to 18 Sv for most latitudes. The modeled overturning is larger than in earlier model versions (Müller et al., 2005) where a lower diapycnal diffusivity has been applied. North Atlantic Deep Water (NADW) is now propagating a little too deep. A weak modeled overturning cell in the deepest part of the Atlantic corresponds to AABW. The value of the transport from the AABW is lower than estimates, which suggests a transport up to 8.5 Sv (Talley et al., 2003). In the South Pacific, the northward flow of AABW takes place below 2,000 m and maximum deep overturning is 14 Sv, comparable to the estimate by Talley et al. (2003) of 13 Sv. Deep equatorial upwelling in the Pacific is with about 9 Sv likely too much and results in nutrient trapping in the thermocline of the equatorial Pacific (not shown). The formation of North Pacific Intermediate Water (NPIW) is rather strong compared to observations (Talley et al., 2003), and propagates too deep. Although most of the Pacific deepwater is supposed to flow southwards again at intermediate depths, too high radiocarbon values at the surface of the North Pacific compared to observations (not shown) may indicate too little upwelling of old water masses here. Deep convection occurs mainly in the North Atlantic south of Greenland and in the Ross and Weddell Sea next to Antarctica. Compared to the standard Bern3D model as used in earlier studies, the Bern3D/PISCES simulates more overturning and younger water masses. As far as the marine biological cycle is concerned, we expect too much biological production and too much nutrient trapping in the Equatorial Pacific due to upwelling.

4.2 $CaCO_3$ production

The spatial pattern of $CaCO_3$ production modeled with the calcite-only version CALMIC1 (Fig. 3a) shows the major large-scale features of the observations (Iglesias-Rodriguez et al., 2002a; Balch et al., 2007). Values are low in the ocean gyres and high in the North Atlantic, North Pacific, and Southern Ocean, as well as in the near coastal upwelling zones in the eastern Pacific and eastern South Atlantic. However, whereas the estimates from satellite images show little calcification in lower latitudes compared to higher latitudes, a larger part of the total modeled calcification occurs in low-latitude upwelling areas. At least for the Equatorial Pacific, this may be linked to model deficiencies as mentioned in the previous

section. The modeled annual average calcification reaches about 12 g C m^{-2} y^{-1} (~1 mg C m^{-3} d^{-1}) in the areas with maximum concentrations of nanophytoplankton. In the North Atlantic, the model simulates annual average calcification rates of between 0.2 and 0.5 mg C m^{-3} d^{-1}. For comparison, Balch et al. (2007) report typical calcification rates of about 4-5 mg C m^{-3} d^{-1} in the North Atlantic in June, but much lower values during other months of the year. The estimated total annual average calcification of Balch et al. (2007) is higher (1.6 Pg C y^{-1}) than in our model (~1.0 Pg C y^{-1}).

In regions away from the coast, differences in modeled $CaCO_3$ production are relatively small between the different model versions (Fig. 3). In other words, $CaCO_3$ production by nanophytoplankton and by mesozooplankton has a similar spatial pattern, as seen in Fig. 4. This reflects the dependency of mesozooplankton on the availability of nanophytoplankton as a source of food. Mesozooplankton graze on nanophytoplankton, in addition to grazing on diatoms, microzooplankton and POC. In near-coastal areas, the $CaCO_3$ production is, however, substantially higher in the versions CALARAG and CAL2ARAG where 1/3 and 2/3 of the production are related to mesozooplankton (Fig. 3). Zonally-averaged production is higher in the Southern Ocean (< 50^{o}S) and for the maximum south of the equator for the version with mesozooplankton calcification (CALARAG, CAL2ARAG) than for the versions with $CaCO_3$ production by nanophytoplankton only (Fig. 5a). This reflects the relatively higher aragonite and meso-calcite production in these productive regions, caused by the relatively higher abundance of mesozooplankton than nanophytoplankton here (Fig 4b). The model versions with no dependency of $CaCO_3$ production on saturation state broadly follow similar zonal patterns.

Observations and estimates of pteropod and foraminifera calcification are scarce. Most of the aragonite production occurs in subpolar and polar areas (Lalli and Gilmer, 1989). Sediment trap studies have shown that in the Southern Ocean, south of the Polar Front, pteropods are the major source of the carbonate flux (>50%) to the depth (Hunt et al., 2008). In the Sub-Antarctic Zone, tests from coccolithophores and foraminifers dominate the flux (Honjo et al., 2000; Honjo, 2004). The model versions with aragonite both provide quite high $CaCO_3$ production rates in polar and subpolar areas, coherent with literature reporting that aragonite shells of pteropods are especially abundant here (e.g. Collier et al., 2000; Honjo et al., 2000; Urban-Rich, 2001; Accornero et al., 2003). However, compared to the high latitudes, the model simulates a higher aragonite production in lower latitudes. While studies report that pteropods are also significant contributors to the $CaCO_3$ flux in low latitudes, such as in the

Indian Ocean (Panchang et al., 2007) and the Equatorial Atlantic (Volbers et al., 2001), the highest biomass of pteropods is expected to be found in cold, high-latitude waters (Lalli and Gilmer, 1989). This may indicate an underestimation of aragonite production in high latitudes or an overestimation in low latitudes by the Bern3D/PISCES model. Since aragonite production is linked to the modeled mesozooplankton distribution, a bias in the latter could explain the latitudinal trend. Figure 5b shows the zonal average modeled distribution of mesozooplankton compared to a data set from the National Marine Fisheries Service (NMFS), compiled by Buitenhuis et al. [2006]. The dataset has a global, yet temporally sparsely resolved coverage and includes samples taken over the top 200 meters. While the overall pattern of spatial variability displayed by the observations is reproduced, the model underestimates the global mesozooplankton concentrations from the dataset, and especially in the North. The global average value of the model equals 0.46 mmol m^{-3}, compared to 0.84 mmol m^{-3} from the NMFS data set. The model shows a better match to observations from the Continuous Plankton Recorder survey (CPR) (Buitenhuis et al., 2007), which are taken from regular surveys in the North Atlantic Ocean only, and are therefore not shown. The average value of the model in this region equals 0.65 mmol m^{-3}, compared to 0.60 mmol m^{-3} from the CPR data set. The improved fit might be due to the better data coverage provided by a time-series type of survey as the CPR, compared to a sparse and synoptic data set like NMFS. The mismatch in the North when comparing to the NMFS dataset suggests that the under/overestimation of aragonite production in the high/low latitudes may be linked to a bias in the modeled mesozooplankton distribution. The parameterization of aragonite production does not include a dependency on temperature, making the missing temperature effect another likely explanation of the he latitudinal trend with higher average rates of aragonite production occurring at low latitudes.

$CaCO_3$ production is simulated down to a depth of ~500 m with little differences in basin-averaged production profiles between the different model versions (Fig. 6a). Most of the production is simulated above 200 m. While the vertical distribution of coccolithophorids (nanophytoplankton) is function of light and nutrient availability, the vertical migrations of pteropods are not taken into account.

In conclusion, $CaCO_3$ production appears to be reasonably represented in the Bern3D/PISCES model when compared with available observation-based estimates and their uncertainty. Aragonite production is likely overestimated in low and mid-latitude regions compared to high-latitude regions as production is linked to mesozooplankton abundance without

considering that many aragonite producing species are found predominantly in cold, high-latitude waters.

4.3 Alkalinity and DIC

The observed spatial patterns of DIC and alkalinity in the surface ocean are well matched by the model (Figs. 5c and d, 7a and b and 8a-d). The Bern3D/PISCES reproduces the high alkalinity values in the north and south Atlantic and the high DIC concentrations in the Southern Ocean. However, the surface alkalinity and DIC concentrations are on average lower than observed. DIC and alkalinity are slightly higher in the versions including aragonite production and dissolution. This is due to the 50% higher solubility of aragonite compared to calcite, which increases shallow dissolution and thus the alkalinity and DIC concentrations at the surface and in the upper part of the water column. Consequently, including aragonite in the model improves the simulated concentrations of surface alkalinity and DIC (Fig. 5c and d).

At depth, the model generally reproduces observation-based alkalinity and DIC patterns (Figs. 7a and b). Existing mismatches can be explained by deficiencies in the simulated ocean circulation. DIC and alkalinity increase along the deep ocean transport path, due to the water column remineralization of organic carbon and $CaCO_3$. Modeled DIC concentrations in most of the Atlantic are low compared to observations and for all model versions. This is likely related to the large formation rate and deep penetration of relatively carbon poor NADW. High DIC and alkalinity concentrations are found in the very deep Atlantic, which is partly linked to the too weak AABW spreading in the Atlantic. The substantial trapping of alkalinity in the deep Atlantic contributes to the low alkalinity concentrations modeled in the deep Pacific as the total ocean alkalinity inventory is fixed. Modeled alkalinity and DIC are higher than observations in the intermediate (~1,000 – 2,000 m) Pacific as expected from the modeled large equatorial upwelling.

The alkalinity and DIC concentrations at depth are slightly improved in the versions including aragonite, due to the rearranging of DIC and alkalinity concentrations in the water column caused by shallow water aragonite dissolution (Fig. 6b). An exception is the alkalinity in the deep Atlantic and Pacific, which is more over- and underestimated, respectively, in the model versions including aragonite (Fig 7a). The differences between the model versions with calcite only and the model versions including aragonite appear in the Taylor diagram (Fig. 9), where

modeled global alkalinity and DIC are compared to pre-industrial values from the Global Ocean Data Analysis Project (GLODAP) (Key et al., 2004). Due to the mismatches in the deep Atlantic and Pacific, the correlation coefficient *r* between modeled and data-based alkalinity is ~ 0.8 for the versions without aragonite, and ~ 0.7 for the versions including aragonite. For DIC, the correlation coefficient is higher than 0.9 for all versions and independent of the form of $CaCO_3$, whereas the standard deviation becomes closer to unity when aragonite is included. To conclude, except for some discrepancies in the Atlantic and Pacific mainly related to deficiencies in modeled circulation, the observed alkalinity and DIC concentrations are fairly well represented by the model.

4.4 Saturation state

Modeled surface CO_3^{2-} concentrations, calcite and aragonite saturation state compare well with observations (Figs. 5e and f, 8e and f). The modeled surface saturation state is on average slightly too high.

At depth, the observed values of aragonite saturation state are relatively well represented in the Southern and Indian Ocean (Figs. 7c, 10e-h), with aragonite saturation horizons around the depth of 1,000 m. Mismatches between model results and observations in the Atlantic and Pacific deep ocean are linked to deficiencies in the modeled DIC and alkalinity fields. Due to these mismatches, a model-observation comparison of the exact depth of the saturation horizons with respect to calcite and aragonite results in low correlations in the Taylor diagram (Fig. 9). However when comparing the patterns between modeled Ω_A and GLODAP observations, the diagram shows correlation coefficients of about 0.95 for all versions and a relative standard deviation just above unity. This indicates an overall good representation of the aragonite saturation state in the Bern3D/PISCES.

4.5 Global carbonate budgets

Next, the global pre-industrial $CaCO_3$ production, export and dissolution fluxes are discussed in the context of observation-based estimates and compared with those from the NEMO/PISCES model (Tables 1 and 2) (Gehlen et al., 2007 and Gangstø et al., 2008). Total $CaCO_3$ production was tuned to ~1 Pg C yr^{-1} for all versions in agreement with published estimates (Iglesias-Rodriguez et al., 2002b; Lee, 2001; Jin et al., 2006; Berelson et al., 2007; Balch et al., 2007). The modeled $CaCO_3$ export at 100 m (0.8 to 0.89 PgC/yr) is smaller than the net production, because $CaCO_3$ is also produced below 100 m (Fig. 6a). Model export

matches well the estimate by Berelson et al. (2007), but is higher than proposed by Sarmiento et al. (2002).

The pelagic $CaCO_3$ dissolution of all model versions is within the range of estimates of 0.5±0.2 (Feely et al., 2004). The total pelagic $CaCO_3$ dissolution is substantially lower in calcite only versions (CALMIC1 and CALMIC2; ~0.4 Pg C yr^{-1}) than in those with aragonite (CALARAG and CAL2ARAG ; ~0.6 Pg C yr^{-1}). This is related to the higher solubility of aragonite compared to calcite. Including aragonite in the model yields a substantial $CaCO_3$ dissolution in the upper part of the water column compared to the version without aragonite (Fig. 6b, Table 2). This increased shallow water $CaCO_3$ dissolution in CALARAG, compared to CALMIC1 and CALMIC2, matches better with observation-based estimates (Feely et al., 2004; Milliman and Droxler, 1996) and confirms the results found by Gangstø et al. (2008). It also supports the hypothesis that the estimated loss of $CaCO_3$ or excess of alkalinity in the upper part of the water column may be at least partly attributed to aragonite dissolution (Milliman and Droxler, 1996; Berelson et al., 2007) and upward mixing (Friis et al., 2007).

In summary, the global $CaCO_3$ production, export and dissolution fluxes in the Bern3D/PISCES model are comparable to observation-based estimates.

5 Future projections: sensitivity to parameterizations, feedbacks and reversibility

5.1 Atmospheric CO_2 and saturation state

Next, we will present the projected anthropogenic perturbation in the $CaCO_3$ cycle and the evolution of underlying drivers for carbon emission commitment scenarios (e.g. Frölicher and Joos, 2010). Carbon emissions are prescribed up to 2100 according to one of the RCP scenarios and then hypothetically (and unrealistically) set to zero to study the long-term impacts of 21st century emissions on the $CaCO_3$ cycle and CO_2. We will first present results for the high-emission, no climate-policy intervention scenario, before showing the range of scenarios in section 5.4. Note that global warming is not modeled here and production of organic material remains constant throughout the simulation. The changes in $CaCO_3$ production and dissolution are thus only forced by changes in the saturation state with respect to $CaCO_3$. The evolution of $CaCO_3$ production is therefore closely linked to the evolution of the saturation state in the surface ocean (Figs. 11b and 12), which itself closely follows

atmospheric CO_2 (Fig. 11a). The evolution of open water $CaCO_3$ dissolution is influenced by the growing extent of undersaturated water (Fig. 13) and the degree of undersaturation.

Differences in projected changes in CO_2, in surface saturation with respect to calcite (Ω_C) or aragonite (Ω_A) and in the volume of undersaturated water are relatively small between the different model versions (Figs. 11b, 12, and 13). Atmospheric CO_2 increases to almost 1,000 ppm by 2100 for the High scenario. Afterwards, CO_2 decreases only slowly to about 600 ppm by 2500 AD, even though emissions are zero after 2100. Ω_C decreases from about 5.2 to 2.2 and Ω_A from about 3.4 to about 1.4 by the year 2100 and for all versions (Fig. 11b). Saturation increases again afterwards at the surface. Regionally, the largest decrease in saturation is found in the tropics, whereas surface waters in high-latitude become undersaturated with respect to aragonite over the course of this century and remain undersaturated by 2500 under the High scenario (Fig. 12). Undersaturation with respect to aragonite is imminent in the Arctic and becomes also widespread in the Southern Ocean. The evolution of the surface ocean aragonite saturation state projected by model versions CALARAG and NODEPCA (Fig. 12) is close to identical up to the year 2100 and differences are small after 2100. In other words, the overall effect from the decreasing calcification on the saturation state is small.

Following Steinacher et al. (2009) and Frölicher and Joos (2010), we distinguish different classes of saturation with respect to aragonite and compute global changes in the volume occupied by undersaturated and oversaturated water masses as an indicator of whole ocean acidification (Fig. 13). Compared to GLODAP observations, our model correctly simulates the volume occupied by the upper three classes, whereas the model underestimates the volume of undersaturated water (crosses in Fig. 13). The volume of water oversaturated with respect to aragonite decreases from about 60% to only 15% of the ocean volume until 2200. Saturation changes long after emissions have been stopped as anthropogenic carbon continues to invade the slowly ventilated deep ocean. Water that is more than three times supersaturated disappears in the next decades and remains absent until the year 2400 for the High case. This illustrates the long-lasting impacts of anthropogenic carbon emissions.

5.2 $CaCO_3$ production and dissolution

Calcite-only production by nanophytoplankton: Under the High scenario, the $CaCO_3$ production decreases to between 0.79 and 0.82 Pg C yr^{-1} by the year 2100, for most of the calcite-only versions (Fig. 11c). This corresponds to a 20-34% reduction relative to pre-

industrial values. The exception is version CALLIN1 which experiences a reduction in calcification of 66%. In this version the PIC-POC is forced to zero for Ω_C approaching one and the production depends particularly sensitively on saturation over the entire Ω_C-range (Fig. 1a). After 2100, the $CaCO_3$ production increases again, following the increase in saturation state and the decrease in CO_2. By the end of the scenario, at the year 2500, the production in the CALLIN1 version with the most sensitive parameterization has increased to about 0.6 Pg C yr^{-1}, compared to ~0.9 Pg C yr^{-1} for the other 3 calcite-only versions (Fig. 11c). Hence, with the exception of the more extreme linear parameterization, the different calcite parameterizations shown in Fig. 1a, whether linear or functions of a Michaelis-Menten curve, provide similar responses of the calcite production to the simulated perturbation in the saturation state.

The decrease in calcite production projected by the Bern3D/PISCES model of 20-66% confirms results from literature. Gehlen et al. (2007) reported a decrease in production equal to 27% by the end of their scenario, where the atmospheric CO_2 was increased at a rate of 1% per year, which is higher than the rate of increase of the IPCC RCP8.5 scenario selected for this study. It resulted in shorter time duration, and the atmospheric concentration reached a maximum of 1144 ppm after 140 years (compared to 992 ppm in our study). Although not directly comparable due to the differences in the underlying scenario and its duration, we note the agreement with our result for the same parameterization. Heinze (2004) projects a decrease in calcification of approximately 30% at atmospheric CO_2 concentrations equal to 1,000 ppm, when fitting a linear dependency to the $CaCO_3$ production rates as a function of CO_2 reported by Riebesell et al. (2000). Ridgwell et al. (2007) report a larger reduction in $CaCO_3$ export production of about 60% at an atmospheric CO_2 content equal to 1,000 ppm. This reduction value is comparable to our estimate obtained for the linear parameterization forced to the intercept (Lin1). While the parameterization Lin1 provides a poor fit to the data and should be viewed as an extreme end-member for the sensitivity study, such a strong response of calcification on saturation state can a priori not be ruled out based on Ridgwell et al. (2007). Based on available evidence, a global decrease in pelagic carbonate production of about 30% in response to ocean acidification under a business-as-usual-scenario (without climate change) seems likely by the year 2100. However, uncertainties in these estimates are large.

Calcite and aragonite production by zooplankton and by nanophytoplankton: The two versions including aragonite, CALARAG and CAL2ARAG, generally yield a larger decrease

in $CaCO_3$ production (Fig. 14) than the versions with calcite only (Fig. 11c). The total $CaCO_3$ production (calcite and aragonite) decreases by 35 and 31% within the year 2100 for the versions CALARAG and CAL2ARAG, respectively (Table 3). By the year 2500, the production has reached 0.80 and 0.78 Pg C yr^{-1}, respectively, corresponding to a 19 and 18% decrease compared to pre-industrial times. The larger reduction in $CaCO_3$ production of the versions including aragonite is caused by the higher solubility of aragonite particles compared to calcite particles. The aragonite saturation state is lower than the calcite saturation state already at pre-industrial times (Fig. 11b) and it decreases to even lower values with increasing atmospheric CO_2.

The different parameterizations for calcite and aragonite production imply different changes in the amount of $CaCO_3$ produced per unit change in the saturation state (Fig. 1b) For $\Omega_C > 4$, the calcite production parameterization LIN1 is by far the most sensitive to changes in the saturation. MIC1 becomes most sensitive for Ω_C below 2.5. The sensitivity of aragonite production to changes in saturation state is comparably low. Preindustrial zonal average surface values for Ω_C were lying within the range of 2.5-6.5. This implies that the model version with parameterization LIN1 will show stronger reductions in $CaCO_3$ compared to other versions at least as long as Ω_C remains above 2.5.

Next to the shape of the relationship between seawater saturation state and pelagic carbonate production, the functional group to which it is assigned, as well as the particular $CaCO_3$ polymorph produced are at the origin of uncertainties in model projections. Since the sensitivity study discussed above demonstrated an overall low sensitivity of the carbonate cycle to the shape of the parameterization, a linear curve to describe the response of calcifying mesozooplankton to decreasing saturation state appears justified at this time. Future studies will provide insight into the calcification mechanism and its controls, thereby enabling the derivation of improved model parameterizations. By including the more soluble aragonite, as well as calcite producing mesozooplankton, we increase the sensitivity of $CaCO_3$ production to increasing atmospheric CO_2.

The Bern3D/PISCES model version CALARAG (calcite produced by nanophytoplankton and aragonite by mesozooplankton) projects a larger reduction in total $CaCO_3$ production (-35%) by the year 2100 than obtained with the NEMO/PISCES model (- 19%). While the latter assumed a Michaelis Menten (MIC2) type dependency of $CaCO_3$ production on seawater saturation state for calcite and aragonite (Gangstø et al., 2008), a linear parameterization was used for aragonite production as a function of Ω_a in the model version CALARAG along with

parameterization MIC1 for calcite. The linear parameterization ARAG has a stronger sensitivity to changes in Ω_a compared to MIC2 for $\Omega_a > 5.5$ (Fig. 1b). Pre-industrial values of Ω_a remained below that threshold in both models, implying an increasing higher sensitivity of aragonite production to changes in Ω_a in NEMO/PISCES with progressing ocean acidification. The opposite holds for calcite production with parameterization CAL1 being more sensitive than CAL2. The stronger response of the Bern3D model reflects the combination of (i) differential sensitivities of parameterizations, differences in (ii) the modeled pre-industrial saturation horizon and (iii) the rate of transfer of anthropogenic CO_2 from the surface to the deep ocean (ventilation, deep convection). Differences in the emission scenarios, scenario RCP8.5 yields atmospheric CO_2 levels about 165 ppm higher by the year 2100 than SRESA2 (Gangstø et al. (2008), most likely play a minor role. The substantial differences obtained with the same biogeochemical model, but coupled to different ocean general circulation models highlights the need for a systematic model inter-comparison study.

$CaCO_3$ dissolution: The absolute magnitude of $CaCO_3$ dissolution in the open water column (Fig. 11d) depends (i) on the amount of $CaCO_3$ produced (Fig. 11c), and (ii) on the saturation state with respect to $CaCO_3$ in the thermocline and deep ocean (Fig. 13). The relative importance of the two factors is quantified with the help of simulations that do not include a dependency of the $CaCO_3$ production on the saturation state. In these simulations, labeled "NODEP", production remains constant and changes in dissolution are entirely driven by changes in the dissolution rate (Eq. (2)).

Global $CaCO_3$ dissolution in the open water increases to reach a plateau after 2200 in the NODEP cases for the High scenario (Fig. 11d). The evolution in dissolution roughly parallels the increase in the volume of undersaturated water (Fig. 13). The evolution in global open water dissolution is more complex in the versions that include the dependency of production on saturation. Global $CaCO_3$ dissolution is projected to decrease until 2100 in response to decreased $CaCO_3$ export. Then, open water dissolution increases and raises well above the pre-industrial level, mainly in response to decreasing deep ocean saturation. The relative dissolution (Fig 11e), i.e. the ratio between open water dissolution to production, increases first gradually until the year 2100, then rapidly until the year 2200, followed by a slight trend to reach ~90-95% for all versions. In other words, the fraction of $CaCO_3$ that is dissolved in the open water increases from pre-industrial ~40% for the calcite-only versions and ~60% for the versions including aragonite to almost 100%. Obviously, the expansion of the volume of undersaturated water with respect to aragonite from pre-industrial 40% to around 80% (and

with respect to calcite from pre-industrial 20% to 60%) of the total ocean volume causes a corresponding increase in open water $CaCO_3$ dissolution. Trends in production and dissolution are getting smaller towards 2500, but the system is still away from equilibrium by the end of the simulation as expected from the century to multi-millennial perturbation life time of an anthropogenic CO_2 perturbation.

5.3 CO_2 – $CaCO_3$ production/dissolution feedback on atmospheric CO_2

In the following, we will quantify the CO_2 – $CaCO_3$ production/dissolution feedback with respect to changes in $CaCO_3$ production only by taking the difference between a model version that includes a dependency of $CaCO_3$ production on saturation state and the corresponding version (NODEP) that does not incorporate such a dependency.

The feedback responses in atmospheric CO_2 are -2.5 to -11.4 ppm by 2100 for the High scenario(Table 3). Thus, the feedback is small compared to the total atmospheric CO_2 perturbation of about 710 ppm by the year 2100, despite a decrease in $CaCO_3$ production of between 20 and 66% in the different versions. The feedback increases after year 2100, although emissions have been set to zero and $CaCO_3$ production increases again (Fig. 11c). This increase is linked to the slow time scale of surface-to-deep transport in the ocean, and the complex interplay between tracer transport, production, and shallow dissolution of $CaCO_3$. Both model versions with aragonite, CALARAG and CAL2ARAG, provide a feedback on the atmospheric CO_2 of -5.8 ppm by the year 2100. The further evolution is also similar between the two versions. After the peak around year 2200 follows a reduction in feedback towards the year 2500, which is stronger than in the versions with calcite only. This reflects a faster recovery of the carbonate system when aragonite is considered, due to the higher solubility of aragonite compared to calcite. By the year 2500, most model versions provide a feedback effect due to decreasing calcification of between -5.1 an -10.9 ppm. The more extreme parameterization (Lin1) yields a stronger CO_2 – $CaCO_3$ production/dissolution feedback corresponding to -24.3 ppm by this time. The feedback effects of the model versions with aragonite, CALARAG and CAL2ARAG, correspond to -6.8 and -6.0 ppm, respectively.

Our results fall in a narrow range considering the variety of model parameterizations and emission scenarios addressed in this study. They range from -3 to -11 ppm by the year 2100, in the case of continuous CO_2 emissions up to the year 2100. Our results compare well to previous studies which report negative feedbacks to atmospheric CO_2 extending from -2 to -12 ppm integrated over the duration of the simulations (Heinze, 2004; Gehlen et al., 2007;

Ridgwell et al., 2007; Hofmann and Schellnhuber, 2009). Despite the diversity in model systems, scenarios and parameterizations all studies converge to project a rather modest negative CO_2 – $CaCO_3$ production/dissolution feedback to increasing atmospheric CO_2.

In order to estimate the potential upper limit of the CO_2 – $CaCO_3$ feedback, calcification was set to 0 after the year 2000 for all model versions (Fig. 15a). While the previous simulations resulted in a maximum feedback of -11 ppm with the strongest parameterization LIN1 by the year 2100, the equivalent maximum CO_2 – $CaCO_3$ feedback when the calcification is set to 0 after 2000 corresponds to -30 ppm (Fig 15b).

The two model versions including aragonite show a very similar response to increasing atmospheric CO_2 despite the very different parameterizations for calcite production. In both version, two thirds of total $CaCO_3$ production are in the form of calcite at steady state. However, in the model version CALARAG calcite is produced by nanophytoplankton only, whereas in the model version CAL2ARAG half of the calcite production is by nanophytoplankton and half by mesozooplankton at steady state. The similar response of the two versions in scenarios with increasing CO_2 is most likely explained by the fact that the abundance of zooplankton is coupled to the food source, i.e., phytoplankton, and that the sensitivities of the different parameterizations of calcite production to saturation state changes are relatively similar. This study suggests that at present and considering the still limited experimental evidence on which to draw for improved process parameterizations, the first order biogeochemical response of the open ocean $CaCO_3$ cycle is adequately reproduced by a model including one calcifying plankton functional type.

PISCES includes only an indirect approach to the ballast effect, by assuming that 50% of the organic matter of the calcifiers is associated with the shell. Since calcite is significantly denser than organic matter, 50% of the biomass of dying calcifiers is routed to the fast sinking POC. A reduction of calcifying nanophytoplankton goes along with a reduction of its contribution to the pool of fast sinking POC. Mesozooplankton contributes to the same pool of fast sinking particles, but as their total biomass is not affected by acidification, there will be no effect of decreasing aragonite production on POC fluxes. The model most likely underestimates the decrease in ballasting of organic C fluxes by $CaCO_3$ (Armstrong et al., 2002; Klaas and Archer, 2002) as a direct consequence of ocean acidification. A reduction in the ballast effect would decrease the penetration depth of organic C. The resulting shallower remineralization depth of organic C would provide a positive feedback to atmospheric CO_2, which might well be of similar or larger magnitude as the CO_2 – $CaCO_3$ production/dissolution feedback

(Barker et al. 2002; Heinze et al, 2004; Hofmann and Schnellnhuber, 2009, Kwon et al., 2009).

Climate change, with higher temperatures is at the origin of an increase in stratification of the ocean waters. Chemical changes related to the temperature effect (decreasing solubility of CO_2 with increasing water temperature), but also a slowing down of the surface to deep transport of water masses, combine to a positive feedback to the atmospheric CO_2 (Joos et al., 1999; Greenblatt and Sarmiento, 2004; Friedlingstein et al., 2006; Plattner et al., 2008.).

Impacts of climate change on saturation are small except in polar waters. The decrease in Ω_A in the Arctic is amplified by surface freshening and sea ice retreat which may cause increased uptake of anthropogenic carbon (Steinacher et al., 2009). Going along with the projected increase in stratification may be a reduction in marine net primary productivity and export production (Steinacher et al., 2010). The reorganization of surface ocean ecosystems with a shift from diatoms towards nanophytoplankton (Bopp et al., 2006) has also been suggested. The ultimate fate of $CaCO_3$ production will thus depend on the interplay between ocean acidification and direct climate change effects. While this discussion highlights the large uncertainties still linked to projections of changes in the marine carbonate cycle and associated feedbacks to atmospheric CO_2, it also suggests that the magnitude of published feedback estimates might represent an upper limit on time scales of decades to a few centuries.

5.4 Sensitivity to future CO_2 emissions

This section addresses the sensitivity of the marine carbonate cycle to projected atmospheric CO_2 trajectories. We focus on the legacy of historical and future CO_2 emissions in terms of impacts on the production/dissolution of marine carbonates (Figs. 16c and d), as well as on the surface ocean saturation state with respect to aragonite (Fig. 16b). To this end we compare the business-as-usual IPCC scenario RCP8.5 (referred to as High) to the alternative pathway RCP6 (Medium) and to a Low scenario. For the High scenario, total cumulative CO_2 emissions of 1916.9 Pg C between 2007 and 2100 translate into a maximum of atmospheric CO_2 of 992 ppm in the year 2100 (Fig. 16a). Atmospheric CO_2 peaks at 702 ppm in 2100 for the Medium scenario (with total cumulative CO_2 emissions of 1138.0 Pg C for the period 2007-2100). In contrast to the High and Medium cases for which emissions increase up to the year 2100 and are then set to zero, the emissions are set to zero after the year 2007 for the Low scenario.

Plotting surface ocean saturation state, $CaCO_3$ production, respectively dissolution as a function of atmospheric CO_2 allows identifying time lags in the system response to the perturbation. The saturation state with respect to aragonite closely follows atmospheric CO_2 (Fig. 16b) suggesting it to be approximately in equilibrium with atmospheric forcing. We observed a small shift towards lower values of the saturation state at identical atmospheric CO_2 values before and after 2100 attributed to the ongoing uptake of CO_2 by the ocean and related changes in carbonate chemistry.

In order to relate changes in surface ocean saturation state with respect to aragonite to habitat suitability for calcifiers, we follow the classification proposed by Kleypas et al. (1999) for tropical coral ecosystems and applied by others at the scale of the global ocean (Steinacher et al., 2009; Frölicher and Joos, 2010). Following this scheme and in terms of carbonate chemistry, $\Omega_A > 4$ stands for optimal, $3 < \Omega_A < 4$, for adequate conditions. While $2 < \Omega_A < 3$ and $1 < \Omega_A < 2$ are indicative of a marginal, respectively inadequate carbonate chemistry for coral growth. Finally values of $\Omega_A < 1$ indicate undersaturated conditions and hence an unsuitable environment for most calcifiers (e.g. pteropods). We stress that uncertainties with ecosystem impacts are large. The high case scenario projects large and, over the duration of the simulation, irreversible changes in surface ocean saturation state. “Suitable habitats” for aragonite producing pelagic organisms such as pteropods ($3 < \Omega_A > 4$) are lost and conditions remain at “best marginal” ($2 < \Omega_A < 3$) by the year 2500. Our model results further confirm the early onset and persistence of undersaturation of high latitude waters (Orr et al., 2005; Steinacher et al., 2009). The evolution of Ω_A is projected to be less severe in the medium case emission scenario. While carbonate chemistry shifts towards “marginal conditions” for the development of pteropods around 2100, the saturation state of low latitude waters increases back to values above 3 by the year 2500. Similarly, the extension and duration of undersaturation in high latitude regions is less severe. Keeping in mind the scarcity of data on consequences of large decreases in saturation state for calcifying organisms and from a safety principle, only the low emission scenario allows for moderate changes in Ω_A and hence the prevalence of suitable conditions for pteropods. The evolution of ocean saturation state with respect to aragonite projected by the Bern3D/PISCES model is consistent with simulations with the comprehensive NCAR climate-carbon cycle model and we refer to the literature for a further discussion on changes in the saturation state and the reversibility of the impacts of 21st century emissions on the carbon cycle and climate (Frölicher and Joos, 2010, Steinacher et al., 2009).

As the atmospheric CO_2 increases, the global mean $CaCO_3$ production decreases at the same rate for all three emission scenarios, until the peak CO_2 values of 992 ppm (High), 702 ppm (Medium) and 342 ppm (Low) are reached. Thereafter, the production increases following nearly the same curves back towards, but without reaching, the original $CaCO_3$ production values. This is a direct consequences of the still higher pCO_2 levels in 2500 and hence the lower surface ocean saturations. The dissolution decreases steadily with increasing atmospheric CO_2 due to the reduced supply of $CaCO_3$ particles (Fig. 16c), also increasing again after the peak of atmospheric CO_2 is reached. However, it increases at a larger rate than it decreased and the dissolution rate by the year 2500 becomes much higher than it was initially. While the global mean dissolution rate was around 0.6 Pg C yr^{-1} at the start of the scenarios, it reaches between 0.65 (Low) and 0.75 (Medium and High) Pg C yr^{-1} by the end of the scenario. This non-linearity occurs because, contrary to the $CaCO_3$ production, the $CaCO_3$ dissolution takes place in the deep ocean. Whereas the surface ocean CO_2 concentration is nearly in equilibrium with the atmospheric CO_2, the deep ocean chemistry recovers much more slowly from the CO_2 perturbation (Fig. 16e).

The resulting feedbacks on atmospheric CO_2 for the 3 scenarios are given in Table 3. Compared to the High scenario which provides a reduction in atmospheric CO_2 of about 5.7 ppm by the year 2100 and 6.8 ppm by the year 2500 due to decreasing calcification and increasing dissolution, the Medium and Low scenarios produce the respective negative CO_2 – $CaCO_3$ feedbacks on atmospheric CO_2 of -4.1 and -1.3 ppm by the year 2100, and -5.0 and -0.8 ppm by the year 2500.

Figure 16 presents the evolution of surface ocean Ω_A (annual mean) with time for the Medium and Low CO_2 emission scenarios and with the CALARAG model version. In the Medium scenario (Fig. 17a), the undersaturation starts in Arctic and the Southern Ocean and is only slightly later than with the High scenario. Although a much smaller area of the higher latitudes become undersaturated, the undersaturation in Arctic is maintained for several centuries in both the High and Medium scenario. The Low scenario provides oversaturation everywhere in the surface areas. With this scenario, the surface waters start to recover already soon after the year 2,000 when the saturation state of the surface waters slowly returns towards near-pre-industrial values. However, even with the Low scenario, the pre-industrial values are not reached within the year 2500 in most regions. In line with other studies (e. g. Frölicher and Joos, 2010), the results indicate that future anthropogenic CO_2 emissions may lead to irreversible changes in Ω_A for several centuries.

6 Conclusions

In this study we used the new biogeochemical Bern3D/PISCES model to explore the sensitivity of the ocean carbon cycle to increasing concentrations of atmospheric CO_2. With a range of sensitivity studies, we explore the effect of i) using different parameterizations of $CaCO_3$ production fitted to available laboratory and field experiments, of ii) letting calcite and aragonite be produced by auto- and heterotrophic plankton groups, and of iii) using CO_2 emissions from the range of the most recent IPCC Representative Concentration Pathways (RCP). Under a high-emission scenario, the $CaCO_3$ production of all the model versions decreases from ~1 Pg C yr^{-1} to between 0.36 and 0.82 Pg C yr^{-1} by the year 2100. By the year 2500, the ratio of open water $CaCO_3$ dissolution to production stabilizes at a value that is 30-50% higher than at pre-industrial times when carbon emissions are set to zero after 2100. From the variety of parameterizations and model versions, the changes in $CaCO_3$ production (and dissolution) resulting from ocean acidification provide only a small overall negative feedback on the atmospheric CO_2 equal to about -11 ppm by the year 2100. The similar response to increasing atmospheric CO_2 by the model version with calcite produced by nanophytoplankton and the one with calcite produced by mesozooplankton may indicate that either of the two plankton groups may be used when simulating future changes in marine pelagic calcification if changes in calcite production in response to environmental drivers are indeed similar for nano- and mesozooplankton. Moreover, in the light of the uncertainties associated with the response of calcifying organisms and the overall similar feedback strengths yielded by the different model versions, the biogeochemical response of the pelagic $CaCO_3$ cycle to ocean acidification may at present be adequately capture by a model with a single calcifying plankton type (e.g. nanophytoplankton in the standard model setting). The maximum potential limit of the CO_2 – $CaCO_3$ production/dissolution feedback by the year 2100, by setting the calcification to 0 after the year 2000, equals -30 ppm.

We quantified changes in the marine $CaCO_3$ cycle for two emission commitment scenarios in which carbon emissions followed RCP8.5 (High) and RCP6 (Medium) until 2100 and are set to zero after 2100, and one scenario where the emissions are set to zero after the year 2007 (Low). In all simulations, the surface aragonite saturation state decreases in parallel to increasing atmospheric CO_2. The resulting decreases in $CaCO_3$ production and increases in dissolution have a negligible effect on surface ocean carbonate chemistry. Ongoing ocean acidification is thus not buffered by changes in $CaCO_3$ production and dissolution. Under the

High scenario, undersaturation of Arctic and Southern Ocean surface waters is projected within few decades, and is maintained over several centuries. In the Arctic, both the Medium and the High scenario give early and long-term undersaturation. Although undersaturation of the surface waters is overall not reached under the Low scenario, we note that the saturation state remains below pre-industrial levels by the year 2500. The results confirm previous studies (Orr et al., 2005; Steinacher et al., 2009; Froelicher et al., 2010) indicating that future anthropogenic CO_2 emissions may lead to irreversible changes in Ω_A for several centuries.

The projected changes in saturation state and decreasing calcification may have large consequences for marine organisms (Fabry et al., 2008; Guinotte and Fabry, 2008; Raven et al., 2005; Kleypas et al., 2006). When interpreting our results in the light of a classification of surface ocean saturation state with respect to aragonite in terms of suitability to marine calcifiers, both scenarios High and Medium suggest large scale habitat loss to occur within a few decades and prevailing up to several centuries. Following the precautionary principle, only scenarios with low carbon emissions seem recommendable when large scale changes in ocean ecosystems and their functioning are to be avoided.

The legacy of ocean acidification and ongoing CO_2 uptake after the unrealistic shut-down of emissions after 2100 is also seen in the deep ocean. The volume of undersaturated water masses remains superior to its pre-industrial value by the year 2500. As a consequence of the slow recovery of the deep ocean after a CO_2 perturbation, the $CaCO_3$ dissolution of all model versions continues to increase over the scenario. By the end of the High scenario, the $CaCO_3$ dissolution-production ratio has stabilized at a value that is 30-50% higher than its initial value. Changes in $CaCO_3$ production will lead to rain ratio changes, which together with a reduction in $CaCO_3$ sedimentation and burial will modify the marine carbonate cycle for several thousands year. The interaction with marine sediments will ultimately bring the system back to a new equilibrium state (Archer, 2005).

Acknowledgements

The study was supported by the EU projects EUROCANS (511106-2), CARBOOCEAN (511176-2) and EPOCA (FP7/2007-2013; no. 211384), and the Swiss National Science Foundation. We would like to thank Olivier Aumont for providing the PISCES model, Marco Steinacher and Kay Bieri for technical assistance, and Birgit Schneider and an anonymous reviewer for very valuable comments. Thanks to J. Büdenbender, S. Lischka and U. Riebesell for access to unpublished data from their study on pteropods in Kongsfjorden.

References

Accornero, A., Manno, C., Esposito, F., and Gambi, M. C.: The vertical flux of particulate matter in the polynya of Terra Nova Bay. Part II, Biological components, Antarct. Sci. 15 (2), 175-188, 2003.

Archer, D.: Fate of fossil fuel CO2 in geologic time, J. Geophys. Res., 110, C09S05, doi:10.1029/2004JC002625, 2005.

Armstrong, R. A., Lee, C., Hedges, J. I., Honjo, S., and Wakeham, S. G. : A new, mechanistic model for organic carbon fluxes in the ocean based on the quantitative association of POC with ballast minerals, Deep-Sea Res., Part II, 49, 219–236, 2001.

Aumont, O., Maier-Reimer, E., Blain, S. and Monfray, P.: An ecosystem model of the global ocean including Fe, Si, P colimitations, Glob. Biogeochem. Cy., 17(2), GB1060, doi:10.1029/2001GB001745, 2003.

Aumont, O., and Bopp, L.: Globalizing results from ocean in situ iron fertilization studies, Glob. Biogeochem. Cy., 20, GB2017, doi:10.1029/2005GB002591, 2006.

Balch, W., Drapeau, D., Bowler, B., Booth, E.: Prediction of pelagic calcification rates using satellite measurements, Deep-Sea Res., Part II, 54 (5-7), 478-495, 2007.

Barker, S., Higgins, J. A., and Elderfield, H.: The future of the carbon cycle: review, calcification response, ballast and feedback on atmospheric CO_2, Philosophical Transactions: Mathematical, Physical and Engineering Sciences, 361, 1977-1999.

Berelson, W. M., Balch, W. M., Najjar, R., Feely, R. A., Sabine, C., and Lee, K.: Glob. Biogeochem. Cy., 21, GB1024, doi:10.1029/2006GB002803, 2007.

Berger, W. H.: Deep-Sea carbonate: Pteropod distribution and the aragonite compensation depth, Deep-Sea Res., 25, 447-452, 1978.

Berner, R. A.: Sedimentation and Dissolution of Pteropods in the Ocean, in The Fate of Fossil Fuel CO_2 in the Oceans, N. R. Andersen and A. Malahoff, editors., pp 243-260, Plenum Press, New York, 1977.

Berner, R. A. and Honjo, S.: Pelagic sedimentation of aragonite: its geochemical significance, Science, 211, 940-942, 1981.

Bijma, J., Spero, H. J., and Lea, D. W.: Reassessing foraminiferal stable isotope geochemistry: Impact of the oceanic carbonate system (experimental results), in Use of Proxies in Paleoceanography: Examples From the South Atlantic, edited by G. Fischer and G. Wefer, pp 489-512, Springer, New York, 1999.

Bopp L.**,** Aumont O., Cadule P., Alvain, S. and Gehlen, M.: Response of diatoms distribution to global warming and potential implications: A global model study, Geophys. Res. Lett., 32 (19), 10.1029/2005GL019606, 2005.

Bryan, F.: High-latitude salinity effects and interhemispheric thermohaline circulations, Nature, 323, 301–304, 1986.

Buitenhuis, E., Le Quéré, C., Aumont, O., Beaugrand, G., Bunker, A., Hirst, A., Ikeda, T., O'Brien, T., Piontkovski, S., and Straile, D.: Biogeochemical fluxes through mesozooplankton, Glob. Biogeochem. Cy., 20, GB2003, doi:10.1029/2005GB002511, 2006.

Casareto, B. E., Niraula, M. O., Fujimura, H, Suzuki, Y.: Effects of carbon dioxide on the coccolithophorid *Pleurochrysis carterae* in incubation experiments, Aquat. Biol., 7, 59–70, 2009.

Collier, R., Dymond, J., Honjo, S., Manganini, S., Francois, R., and Dunbar, R.: The vertical flux of biogenic and lithogenic material in the Ross Sea: moored sediment trap observations 1996-1998, Deep-Sea Res. II, 47, 3491-3520, 2000.

Comeau, S., Gorsky, G., Jeffree, R., Teyssié, J.-L. and Gattuso, J.-P. : Impact of ocean acidification on a key Arctic pelagic mollusc (*Limacina helicina*), Biogeosciences 6, 1877-1882, 2009.

Delille, B., Harlay, J., Zondervan, I., Jacquet, S., Chou, L., Wollast, R., Bellerby, R. G. J., Frankignoulle, M., Borges, A. V., Riebesell, U., and Gattuso, J.-P.: Response of primary production and calcification to changes of pCO_2 during experimental blooms of the

coccolithophorid *Emiliania huxleyi*, Glob. Biogeochem. Cy., 19, GB2023, doi:10.1029/2004GB002318, 2005.

Denman, K. L., Brasseur, G., Chidthaisong, A., Ciais, P., Cox, P. M., Dickinson, R. E., Hauglustaine, D., Heinze, C., Holland, E., Jacob, D., Lohmann, U., Ramachandran, S., da Silva Dias, P. L., Wofsy, S. C. & Zhang, X.: Couplings between changes in the climate system and biogeochemistry. In: Solomon, S., Qin, D., Manning, M., Chen, Z., Marquis, M., Averyt, K. B., Tignor, M. & Miller, H. L. (eds.), Climate Change 2007: The Physical Science Basis. Contribution of Working Group I to the Fourth Assessment Report of the Intergovernmental Panel on Climate Change (IPCC). Cambridge University Press, Cambridge, United Kingdom and New York, NY, USA, pp. 499-587, 2007.

Dissard, D., Nehrke, G., Reichart, G. J. and Bijma J.: Impact of seawater pCO_2 changes on calcification and on mG/cA and sR/cA in benthic foraminifera calcite (*Ammonia tepida*): results from culturing experiments, Biogeosciences Discuss., 6, 3771-3802, 2009.

Edwards, N. R., Wilmott, A. J. and Killworth, P. D.: On the role of topography and wind stress on the stability of the thermohaline circulation, J. Phys. Oceanogr. 28, 756–778, 1998.

Edwards, N. R. and Marsh, R.: Uncertainties due to transport-parameter sensitivity in an efficient 3-D ocean-climate model, Climate Dyn. 24 (4), 415–433, doi:10.1007/s00382–004–0508–8, 2005.

Fabry, V. J.: Shell growth rates of pteropod and heteropod mollusks and aragonite production in the open ocean: Implications for the marine carbonate system, J. Mar. Res., 48, 209-222, 1990.

Fabry, V. J., and Deuser, W. G.: Aragonite and magnesium calcite fluxes to the deep Sargasso Sea, Deep-Sea Res. Part A. Oceanographic Research Papers, 38 (6), 713-728, 1991.

Fabry, V. J., Seibel, B. A., Feely, R. A. and Orr, J. C.: Impacts of ocean acidification on marine fauna and ecosystem processes, ICES J. Mar. Sci., 65, 414–432, 2008.

Feely, R. A., Sabine, C. L., Lee, K., Berelson, W., Kleypas, J., Fabry, V. J. and Millero, F. J.: Impact of anthropogenic CO_2 on the $CaCO_3$ system in the oceans, Science, 305, 362-366, 2004.

Frankignoulle, M. and Canon, C.: Marine calcification as a source of carbon dioxide: Positive feedback of increasing atmospheric CO_2, Limnol. Oceanogr., 39 (2), 458-462, 1994.

Friedlingstein, P., Cox, P., Betts, R., Bopp, L., von Bloh, W., Brovkin, V., Cadule, P., Doney, S., Eby, M., Fung, I., Bala, G., John, J., Jones, C., Joos, F., Kato, T., Kawamiya, M., Knorr, W., Lindsay, K., Matthews, H. D., Raddatz, T., Rayner, P., Reick, C., Roeckner, E., Schnitzler, K.-G., Schnur, R., Strassmann, K., Weaver, A. J., Yoshikawa, C. and Zeng, N.: Climate-carbon cycle feedback analysis: Results from the C4MIP model intercomparison, J. Climate 19 (14), 3337–3353, 2006.

Frölicher, T. L. and Joos, F.: Reversible and irreversible impacts of greenhouse gas emissions in multi-century projections with a comprehensive climate-carbon model, Clim.Dyn., doi:10.1007/s00382-009-0727-0, in press, 2010.

Gangstø, R., Gehlen, M., Schneider, B., Bopp, L., Aumont, O. and Joos, F.: Modeling the marine aragonite cycle: changes under rising carbon dioxide and its role in shallow water $CaCO_3$ dissolution, Biogeosciences 5 (4), 1057–1072, 2008.

Gattuso J.-P., Frankignoulle, M., Bourge, I., Romaine, S., and Buddemeier, R. W.: Effect of calcium carbonate saturation of seawater on coral calcification, Global Planet. Change, 18, 37-46, 1998.

Gao, K. S., Ruan, Z. X., Villafane, V. E., Gattuso, J.-P., and Helbling, E. W.: Ocean acidification exacerbates the effect of UV radiation on the calcifying phytoplankter *Emiliania huxleyi*, Limnol. oceanogr., 54 (6), 1855-1862, 2009.

Gehlen M., Bopp, L., Emprin, N., Aumont, O., Heinze, C., and Ragueneau, O.: Reconciling surface ocean productivity, export fluxes and sediment composition in a global biogeochemical ocean model, Biogeosciences, 3, 521-537, 2006.

Gehlen M., Gangstø, R., Schneider, B., Bopp, L., Aumont, O., and Ethe, C.: The fate of pelagic $CaCO_3$ production in a high CO_2 ocean: A model study, Biogesciences 4, 505-519, 2007.

Gerber, M., Joos, F., Vazquez Rodriguez, M., Touratier, F. & Goyet, C.: Regional air-sea fluxes of anthropogenic carbon inferred with an Ensemble Kalman Filter, Glob. Biogeochem. Cy. 23, GB1013, doi:10.1029/2008GB003247, 2009.

Gerber, M. and Joos, F.: Carbon sources and sinks from an Ensemble Kalman Filter ocean data assimilation, Global Biogeochemical Cycles, 24/GB3004, 2010.

Griffies, S. M.: The Gent-McWilliams skew flux, J. Phys. Oceanogr., 28, 831–841, 1998.

Godoi, R. H. M., Aerts, K., Harlay, J., Kaegi, R., Ro, Chul-Un, Chou, L., and Van Grieken, R.: Organic surface coating on Coccolithophores - *Emiliania huxleyi*: Its determination and implication in the marine carbon cycle, Microchem. J., 91 (2), 266-271, 2009.

Goyet, C., Healy, R. J., and Ryan, J. P.: Global distribution of total inorganic carbon and total alkalinity below the deepest winter mixed layer depths, ORNL/CDIAC-127, NDP-076, Carbon Dioxide Information Analysis Center, Oak Ridge National Laboratory, U.S. Department of Energy, Oak Ridge, Tennessee, 2000.

Greenblatt, J. and Sarmiento, J.: Variability and climate feedback mechanisms in ocean uptake of CO_2, In: Field, C.B. and Raupach, M.R. (eds) The Global Carbon Cycle: Integrating Humans, Climate, and the Natural World, Scope 62, Island Press, Washington, DC, 257-275, 2004.

Heinze, C.: Simulating oceanic $CaCO_3$ export production in the greenhouse, Geophys. Res. Let., 31, L16308, doi:10.1029/2004GL020613, 2004.

Hofmann, M., and Schellnhuber, H.-J.: Oceanic acidification affects marine carbon pump and triggers extended marine oxygen holes, Proc. Natl. Acad. Sci, 106, 3017–3022, 2009.

Honjo, S., Francois, R., Manganini, S., Dymond, J., and Collier, R.: Particle fluxes to the interior of the Southern Ocean in the Western Pacific sector along 170°W, Deep-Sea Res. II, 47, 3521-3548, 2000.

Honjo S.: Particle export and the biological pump in the Southern Ocean, Antarct. Sci., 16 (4), 501-516, 2004.

Hunt, B. P. V., Pakhomov, E. A., Hosie, G. W., Siegel, V., Ward, P., and Bernard K.: Pteropods in Southern Ocean ecosystems, Progress In Oceanography, 78 (3), 193-221, 2008.

Iglesias-Rodriguez, M. D., Armstrong, R., Feely, R., Hood, R., Kleypas, J., Milliman, J. D., Sabine, C., and Sarmiento, J.: Representing key phytoplankton functional groups in oceanic carbon cycle models: Coccolithophorids, Global Biogeochem. Cy., 16, 1100, doi:10.1029/2001GB001454, 2002a.

Iglesias-Rodriguez, M. D., Armstrong, R., Feely, R., Hood, R., Kleypas, J., Milliman, J. D., Sabine, C., and Sarmiento, J.: Progress made in study of ocean's calcium carbonate budget, EOS, 83(34), 365, 374-375, 2002b.

Iglesias-Rodriguez, M. D., Halloran, P. R., Rickaby, R. E. M., Hall, I. R., Colmenero-Hidalgo, E., Gittins, J. R., Green, D. R. H., Tyrrell, T., Gibbs, S. J., von Dassow, P., Rehm,

E., Armbrust, E. V. and Boessenkool, K. P.:, Phytoplankton calcification in a high-CO_2 world, Science, 320, 336–340, 2008.

Jin, X., Gruber, N., Dunne, J. P., Sarmiento, J. L., and Armstrong, R. A.: Diagnosing the contribution of phytoplankton functional groups to the production and export of particulate organic carbon, $CaCO_3$, and opal from global nutrient and alkalinity distributions, Global Biogeochem. Cy., 20, GB2015, doi:10.1029/2005GB002532, 2006.

Joos, F., Plattner, G.-K., Stocker, T. F., Marchal, O., Schmittner, A.: Global warming and marine carbon cycle feedbacks on future atmospheric CO_2, Science, 284/5413, 464-467,1999.

Jury, C. P., Whitehead, R. F., and Szmant, A. M.: Effects of variations in carbonate chemistry on the calcification rates of Madracis mirabilis (Duchassaing 1861): Bicarbonate concentrations best predict calcification rates, Global Change Biology, accepted, doi: 10.1111/j.1365-2486.2009.02057.x, 2009.

Key, R. M., Kozyr, A., Sabine, C. L., Lee, K., Wanninkhof, R., Bullister, J. L., Feely, R. A., Millero, F. J., Mordy, C., and Peng, T.-H.: A global ocean carbon climatology: Results from Global Data Analysis Project (GLODAP), Glob. Biogeochem. Cy., 18, GB4031, doi:10.1029/2004GB002247, 2004.

Klaas, C. and Archer, D.: Association of sinking organic matter with various types of mineral ballast in the deep sea: Implications for the rain ratio, Glob. Biogeochem. Cy., 16 (4), 1116, doi:10.1029/2001GB001765, 2002.

Kleypas, J. A., Buddemeier, R. W., Archer, D., Gattuso, J.-P., Langdon, C., and Opdyke, B. N.: Geochemical consequences of increased atmospheric carbon dioxide on coral reefs, Science, 284, 118-120, 1999.

Kleypas, J. A., Feely, R. A., Fabry, V. J., Langdon, C., Sabine, C. L., and Robbins, L. L.: Impacts of ocean acidification on coral reefs and other marine calcifiers: A guide for future research, report of a workshop held 18-20 April 2005, St. Petersburg, FL, sponsored by NSF, NOAA, and the U.S. Geological Survey, 88 pp, 2006.

Kuroyanagi, A., Kawahata, H., Suzuki, A., Fujita, K., Irie, T.: Impacts of ocean acidification on large benthic foraminifers: Results from laboratory experiments, Mar. Micropaleontol., In Press, 2009.

Kwon, E. Y., Primeau, F., Sarmiento, J. L.: The impact of remineralization depth on the air-sea carbon balance, Nature Geoscience, 2, 630-635, doi:10.1038/ngeo612.

Lalli, C. M., and Gilmer, R. W.: Pelagic snails: The Biology of Holoplanktonic Gastropod Mollusks, Stanford University Press, 1989.

Langer G., Geisen, M., Baumann, K.-H., Kläs, J., Riebesell, U., Thoms, S., and Young, J. R.: Species-specific responses of calcifying algae to changing seawater carbonate chemistry, Geochem. Geophys. Geosyst., 7, Q09006, doi:10.1029/2005GC001227, 2006.

Langdon, C., Broecker, W. S., Hammond, D. E., Glenn, E., Fitzsimmons, K., Nelson, S. G., Peng, T.-H., Hajdas, I., and Bonani, G.: Effect of elevated CO_2 on the community metabolism of an experimental coral reef, Glob. Biogeochem. Cy., 17(1), 1011, doi:10.1029/2002GB001941, 2003.

Langdon, C., and Atkinson, M. J.: Effect of elevated pCO_2 on photosynthesis and calcification of corals and interactions with seasonal change in temperate/irradiance and nutrient enrichment, J. Geophys. Res., 110, C09S07, doi:10.1029/2004JC002576, 2005.

Legendre, L., and Le Févre, J.: Microbial food webs and the export of biogenic carbon in oceans, Aquat. Microb. Ecol. 9, 69–77, 1995.

Lee, K.: Global net community production estimated from the annual cycle of surface water total dissolved inorganic carbon, Limnol. Oceanogr., 46 (6), 1287-1297, 2001.

Lombard, F., da Rocha, R. E., Bijma, J., and Gattuso, J.-P.: Effect of carbonate ion concentration and irradiance on calcification in planktonic foraminifera, Biogeosciences, 7, 247-255, doi:10.5194/bg-7-247-2010.

Milliman, J. D., and Droxler, A. W.: Neritic and pelagic carbonate sedimentation in the marine environment: ignorance is not bliss, Geol. Rundsch., 85, 496-504, 1996.

Moy, A. D., Bray, S. G., Trull, T. W., and Howard, W. R.: Reduced calcification in modern Southern Ocean planktonic foraminifera, Nature Geoscience, doi:10.1038/ngeo460, 2009.

Müller, S. A., Joos, F., Edwards, N. R. and Stocker, T. F.: Water mass distribution and ventilation time scales in a cost-efficient, three-dimensional ocean model, J. Climate 19 (21), 5479–5499, 2006.

Müller, S. A., Joos, F., Plattner, G.-K., Edwards, N. R. and Stocker, T. F., Modeled natural and excess radiocarbon: sensitivities to the gas exchange formulation and ocean transport strength, Glob. Biogeochem. Cy. 22. GB3011, doi:10.1029/2007GB003065, 2008.

Müller, M. N., Schulz, K. G. and Riebesell, U., Effects of long-term high CO_2 exposure on two species of coccolithophores, Biogeosciences, 7, 1109-1116, 2010.

Najjar, R. G. and J. Orr, J.: Biotic-HOWTO, technical report, 15 pp., Lab. des Sci. du Clim. et l'Environ., Comm. à l'Energie At. Saclay, Gif-sur-Yvette, France (Available at http://www.ipsl.jussieu.fr/OCMIP/phase2/simulations/Biotic/HOWTO-Biotic.html), 1999.

Orr, J., Najjar, R. G., Sabine, C. L. and Joos, F.: Abiotic-HOWTO, technical report, 25 pp., Lab. des Sci. du Clim. et l'Environ., Comm. à l'Energie At. Saclay, Gif-sur-Yvette, France (Available at http://www.ipsl.jussieu.fr/OCMIP/phase2/simulations/Abiotic/HOWTO-Abiotic.html), 1999.

Orr, J. C., Fabry, V. J., Aumont, O., Bopp, L., Doney, S. C., Feely, R. A., Gnanadesikan, A., Gruber, N., Ishida, A., Joos, F., Key, R. M., Lindsay, K., Maier-Reimer, E., Matear, R., Monfray, P., Mouchet, A., Najjar, R. G., Plattner, G.-K., Rodgers, K. B., Sabine, C. L., Sarmiento, J. L., Schlitzer, R., Slater, R. D., Totterdell, I. J., Weirig, M.-F. , Yamanaka, Y., and Yool, A.: Antropogenic ocean acidification over the twenty-first century and its impact on calcifying organisms, Nature, 437, 681–686, 2005.

Panchang, R., Nigam, R., Riedel, F., Janssen, A. W. And Ko Yui Hla, U.: A review of the studies on pteropods from the northern Indian Ocean region with a report on the pteropods of Irrawaddy continental shelf off Myanmar (Burma), Indian J. Mar. Sci., 36(4), 384-398, 2007.

Parekh, P., Joos, F., and Müller, S. A.: A modeling assessment of the interplay between aeolian iron fluxes and iron-binding ligands in controlling carbon dioxide fluctuations during Antarctic warm events, Paleoceanography 23. doi:10.1029/2007PA001531, 2008.

Plattner, G.-K., Knutti, R., Joos, F., Stocker, T. F., von Bloh, W., Brovkin, V., Cameron, D., Driesschaert, E., Dutkiewiz, S., Eby, M., Edwards, N. R., Fichefet, T., Hargreaves, J. C., Jones, C. D., Loutre, M. F., Matthews, H. D., Mouchet, A., Müller, S. A., Nawrath, S., Price, A., Sokolov, A., Strassmann, K. M., Weaver, A. J.: Long-term climate commitments projected with climate - carbon cycle models, Journal of Climate, 21/12, 2721-2751,2008.

Raven, J.A.; Falkowski, P.G.: Oceanic sinks for atmospheric CO_2, Plant Cell Environ. 22, 741-755, doi:10.1046/j.1365-3040.1999.00419, 1999.

Riebesell U., Zondervan, I., Rost, B., Tortell, P. D., Zeebe, R. E., and Morel, F. M. M.: Reduced calcification of marine plankton in response to increased atmospheric CO_2, Nature, 407, 364-367, 2000.

Ridgwell, A., Zondervan, I., Hargreaves, J. C., Bijma, J., and Lenton, T. M.: Assessing the potential long-term increase of oceanic fossil fuel CO_2 uptake due to CO_2-calcification feedback, Biogeosciences, 4, 481-492, 2007.

Ridgwell, A., Schmidt, D. N., Turley, C., Brownlee, C., Maldonado, M. T., Tortell, P. and Young, J. R.: 'From laboratory manipulations to earth system models: predicting pelagic calcification and its consequences', Biogeosciences Discuss., 6 p. 3455-3480, 2009.

Ritz, S. P., Stocker, T. F. and Müller, S. A.: Modeling the effect of abrupt ocean circulation change on marine reservoir age, Earth Planet. Sc. Lett.268 (1-2), 202–211, doi:10.1016/j.epsl.2008.01.024, 2008.

Rowe, G. T., Wei, C., Nunnally, C., Haedrich, R., Montagna, P., Baguley, J.G., Bernhard, J.M., Wicksten, M., Ammons, A., Escobar Briones, E.G., Soliman, and Y., Deming, J.: Comparative biomass structure and estimated carbon flow in food webs in the deep Gulf of Mexico, Deep-Sea Res. II 55, 2699–2711, 2008.

Sarmiento, J. L., Dunne, J., Gnanadesikan, A., Key, R. M., Matsumoto, K., and Slater, R.: A new estimate of the $CaCO_3$ to organic carbon export ratio, Glob. Biogeochem. Cy., 16(4), 1107, doi:10.1029/2002GB001919, 2002.

Schiebel, R.: Planktic foraminiferal sedimentation and the marine calcite budget, Glob. Biogeochem. Cy., 16 (4), 1065, doi:10.1029/2001GB001459, 2002.

Sciandra, A., Harlay, J., Lefèvre, D., Lemée, R., Rimmelin, P., Denis, M., and Gattuso, J.-P.: Response of coccolithophorid *Emiliania huxleyi* to elevated partial pressure of CO_2 under nitrogen limitation, Mar. Ecol.-Prog. Ser., 261, 111-222, 2003.

Shi, D., Xu, Y. and Morel, F. M. M.: Effects of the pH/pCO_2 control method on medium chemistry and phytoplankton growth, Biogeosciences, 6, 1199-1207, 2009.

Siddall, M., Stocker, T. F., Henderson, G. M., Joos, F., Frank, M., Edwards, N. R., Ritz, S. P. and Müller, S. A., Modeling the relationship between $^{231}Pa/^{230}Th$ distribution in North Atlantic sediment and Atlantic meridional overturning circulation, Paleoceanography 22, PA2214, doi:10.1029/2006PA001358, 2007.

Spero, H. J., Bijma, J., Lea, D.W., and Bemis, B. E.: Effect of seawater carbonate concentration on foraminiferal carbon and oxygen isotopes, Nature, 390, 497–500, 1997.

Steinacher, M., Joos, F., Frölicher, T. L., Plattner, G.-K., and Doney, S. C.: Imminent ocean acidification in the Arctic projected with the NCAR global coupled carbon cycle-climate model, Biogeosciences, 6, 515–533, 2009.

Steinacher, M., Joos, F., Frölicher, T. L., Bopp, L., Cadule, P., Cocco, V., Doney, S. C., Gehlen, M., Lindsay, K., Moore, J. K., Schneider, B., and Segschneider, J.: Projected 21st century decrease in marine productivity: a multi-model analysis, Biogeosciences, 7/3, 979-1005, 2010.

Strassmann, K. M., G.-K. Plattner, F. Joos, "CO_2 and non-CO_2 radiative forcings in climate projections for twenty-first century mitigation scenarios", Clim. Dynam., 33/6, 737-749,2009.

Talley, L. D., Reid, J. L., and Robbins, P. E.: Data-based meridional overturning streamfunctions for the global ocean, J. Clim., 16, 3213-3226, 2003.

Tschumi, T., Joos, F. and Parekh, P.: How important are Southern Hemisphere wind changes for low glacial carbon dioxide? A model study, Paleoceanography, 23, PA4208, doi:10.1029/2008PA001592, 2008.

Urban-Rich, J., Dagg, M., and Peterson, J.: Copepod grazing on phytoplankton in the Pacific sector of the Antarctic Polar Front, Deep-Sea Res. II, 48, 4223-4246, 2001.

Volbers, A. N. A.: Planktic foraminifera as paleoceangraphic indicators: Production, preservation, and reconstruction of upwelling intensity, implications from late quarternary South Atlantic sediments. Berichte, Fachbereich Geowissenschaften, Universität Bremen, 184, 114 pp, 2001.

Van Vuuren, D. P., M. Meinshausen, G.-K. Plattner, F. Joos, K. M. Strassmann, S. J. Smith, T. M. L. Wigley, S. C. B. Raper, K. Riahi, F. de la Chesnaye, M. den Elzen, J. Fujino, K. Jiang, N. Nakicenovic, S. Paltsev, and J. M. Reilly, "Temperature increase of 21st century mitigation scenarios ", PNAS, 105/40, 15258-15262,2008.

Wolf-Gladrow, D. A., Riebesell, U., Burkhardt, S., and Bijma, J.: Direct effects of CO_2 concentration on growth and isotopic composition of marine plankton, Tellus, 51B (2), 461-476, 1999.

Zondervan, I., Zeebe, R. E, Rost, B., and Riebesell, U.: Decreasing marine biogenic calcification: A negative feedback on rising atmospheric pCO_2, Glob. Biogeochem. Cy., 15(2) 507-516, 2001.

Zondervan, I., Rost, B., and Riebesell, U.: Effect of CO_2 concentration on the PIC/POC ratio in the coccolithophore *Emiliania huxleyi* grown under light-limiting conditions and different daylengths, J. Exp. Mar. Biol. Ecol., 272, 55-70, 2002.

Zondervan, I.: The effects of light, macronutrients, trace metals and CO_2 on the production of calcium carbonate and organic carbon in coccolithophores - A review, Deep-Sea Res. II, 54, 521-537, 2007.

Table 1. Simulated pre-industrial $CaCO_3$ production (after 3,000 years of integration) for different parameterizations of $CaCO_3$ production in the Bern3D/PISCES model.

Model version	Calcite production ($Pg\ C\ yr^{-1}$)	Aragonite production ($Pg\ C\ yr^{-1}$)	Parameterization of the dependency of $CaCO_3$ production on saturation state
Calcite production by nanophytoplankton only			
CALMIC1	1.0	-	Michaelis-Menten, this study
CALMIC2	1.00	-	Michaelis-Menten based on Gehlen et al. 2007
CALLIN1	1.05	-	Linear curve, forced to zero for Ω=1
CALLIN2	1.04	-	Linear curve, freely fitted
NODEPC	1.02	-	Production is independent of saturation state
Calcite production by nanophytoplankton and aragonite production by mesozooplankton			
CALARAG	0.66	0.34	Michaelis-Menten (this study) for calcite, linear for aragonite
NODEPCA	0.69	0.35	Production is independent of saturation state
Calcite production by nanophyto- and mesozooplankton and aragonite production by mesozooplankton			
CAL2ARAG	0.33 + 0.31	0.34	Michaelis-Menten for calcite by nanoplankton, linear for aragonite production, linear for calcite production by mesoplankton
NODEPC2A	0.36 + 0.35	0.35	Production is independent of saturation state

Table 2. The pre-industrial $CaCO_3$ budget: Results are for different parameterizations of the $CaCO_3$ production in the Bern3D/PISCES model and the NEMO/PISCES model, labeled PISC-CAL (Gehlen et al., 2007), and PISC-ARAG (Gangstø et al., 2008). Parameterizations for the carbonate cycle are comparable between versions CAL-MIC2 and PISC-CAL and between versions CAL-ARAG and PISC-ARAG. The lower boundary represents the deepest model grid boxes. The flux at the lower boundary is not to be compared with estimates of the burial flux; the latter is not modeled in this study. Units are Pg C yr^{-1}.

Parameterization	Bern3D CAL-MIC1	Bern3D CAL-MIC2	Bern3D CAL-ARAG	Bern3D CAL2-ARAG	NEMO PISC-CAL	NEMO PISC-ARAG	Observation-based estimates
Source							
Net $CaCO_3$ production	1.05	1.00	1.00	0.99	0.79	0.87	0.8-1.6[1,2,3,4,5]
Sinks							
Pelagic $CaCO_3$ dissolution	0.40	0.40	0.61	0.60	0.48	0.55	0.5±0.2[6],
(% of tot. $CaCO_3$ production)	(38.1%)	(40.0%)	(61.0%)	(60.6%)	(60.8%)	(63.2%)	1.0±0.5[4] (>1500 m)
$CaCO_3$ flux at lower boundary	0.65	0.60	0.39	0.39	0.31	0.32	-
$CaCO_3$ burial flux	-	-	-	-	-	-	0.3
Related fluxes							
Export flux 100 m	0.80	0.76	0.81	0.83	0.60	0.63	0.6[7], 0.6-1.6[4]
(% of tot. $CaCO_3$ production)	(76.2%)	(76.3%)	(81.0%)	(83.8%)	(75.9%)	(72.4%)	-
Pelagic $CaCO_3$ dissolution 0-1 km, % of tot. production	0.036%	0.036%	26.0%	26.4%	2.5%	14%	60-80%[8]
Pelagic $CaCO_3$ dissolution 0-2 km, % of tot. dissolution	44%	52.3%	71.6%	71.3%	38%	58%	$\geq$ 60%[6]

1. Iglesias-Rodriguez et al. (2002b), 2. Lee (2001), 3. Jin et al. (2006), 4. Berelson et al. (2007), 5. Balch et al. (2007), 6. Feely et al. (2004), 7. Sarmiento et al. (2002), 8. Milliman and Droxler (1996).

Table 3. Sensitivity of $CaCO_3$ production and of the CO_2 – $CaCO_3$ production/dissolution feedback to different parameterizations and emission pathways. Emissions follow the High, Medium and Low scenario over the 21st century and are set to zero after 2100. N = not applicable.

	$CaCO_3$ prod., 1766 (Pg C yr^{-1})	$CaCO_3$ prod., 2100 - 1766 (%)	$CaCO_3$ prod., 2500 - 1766 (%)	Feedback by 2100 (ppm)	Feedback by 2500 (ppm)
Sensitivity to parameterizations (High scenario)					
CALLIN1, calcite	1.06	-66	-42	-11.37	-24.32
CALLIN2, calcite	1.05	-22	-15	-3.60	-8.70
CALMIC1, calcite	1.06	-34	-16	-4.29	-10.85
CALMIC2, calcite	1.01	-20	-08	-2.53	-5.05
CALARAG, calcite	0.66	-32	-16	N	N
CALARAG, aragonite	0.32	-40	-25	N	N
CALARAG, total $CaCO_3$	0.98	-35	-19	-5.77	-6.81
CAL2ARAG, calcite by nanop.	0.34	-31	-15	N	N
CAL2ARAG, aragonite	0.32	-40	-25	N	N
CAL2ARAG, calcite by mesop.	0.30	-21	-14	N	N
CAL2ARAG, total $CaCO_3$	0.96	-31	-18	-5.78	-5.96
Sensitivity to scenarios					
CALARAG, tot. $CaCO_3$, High	0.98	-35	-19	-5.77	-6.81
CALARAG, tot. $CaCO_3$, Medium	0.98	-23	-11	-4.07	-5.01
CALARAG, tot. $CaCO_3$, Low	0.98	-5	-2	-1.26	-0.77

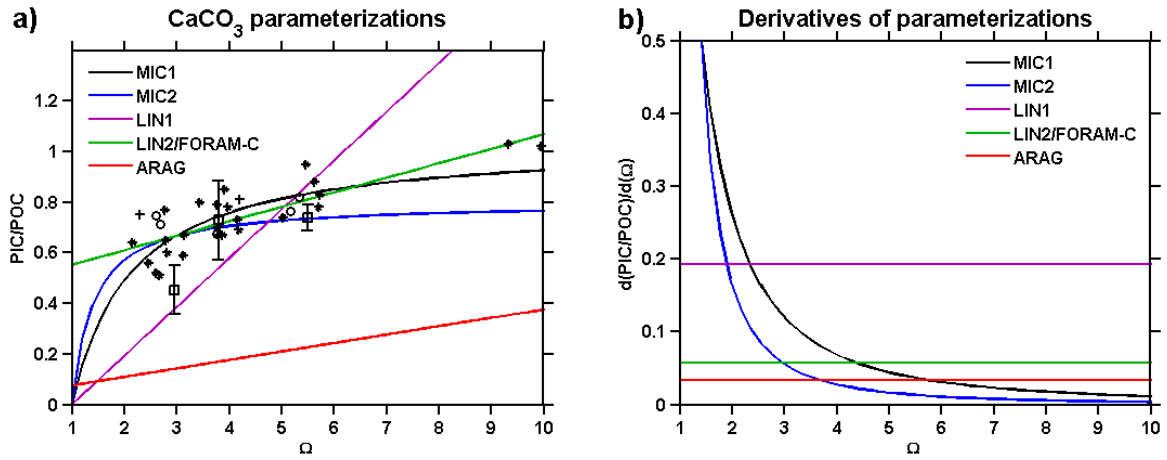

Figure 1. PIC-POC ratio (a) as a function of calcite saturation state with respect to ambient waters. Data from Delille et al. (2005) are shown as black squares with error bars, from Zondervan et al. (2002) as black asterisks, data from Iglesias-Rodriguez et al. (2008) are shown as black circles and data from Shi et al. (2009) as black crosses. Three new parameterizations are fitted to the data and used in the Bern3D/PISCES model to compute $CaCO_3$ production: A Michaelis-Menten curve (MIC1), a linear curve that is forced to go through Ω_C=1 (LIN1) and a linear curve that was freely fitted to the data (LIN2), which is also used for calcite production by mesozooplankton (FORAM-C). In addition, the Michaelis-Menten curve that was used in Gehlen et al. (2007) and Gangstø et al. (2008) is included (MIC2). The red curve denotes the parameterization used for aragonite production (ARAG). The respective sensitivities, d(PIC-POC)/dΩ, are shown in b).

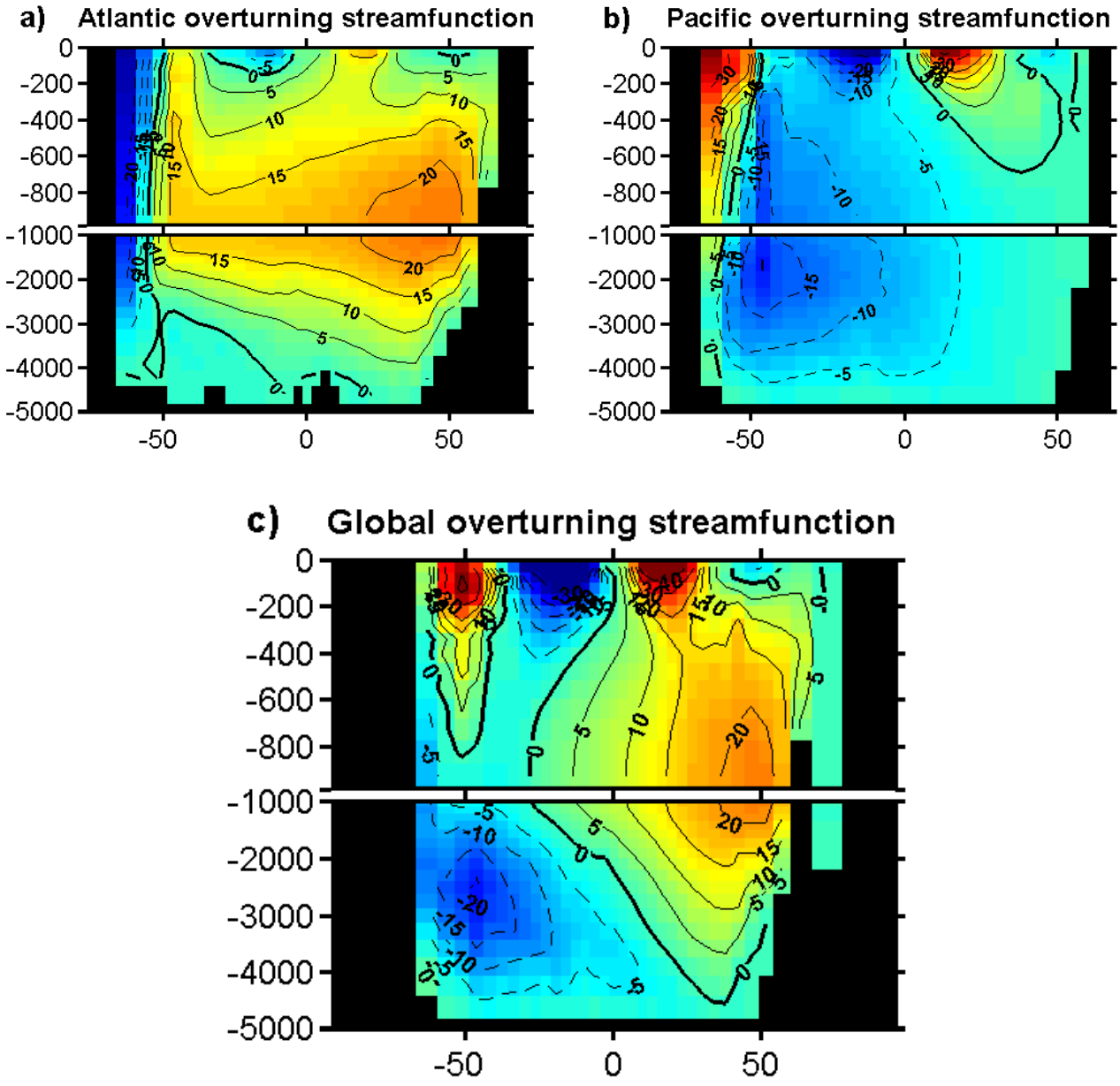

Figure 2. Streamfunction of the Bern3D/PISCES model for the a) Atlantic, b) Pacific and c) global ocean.

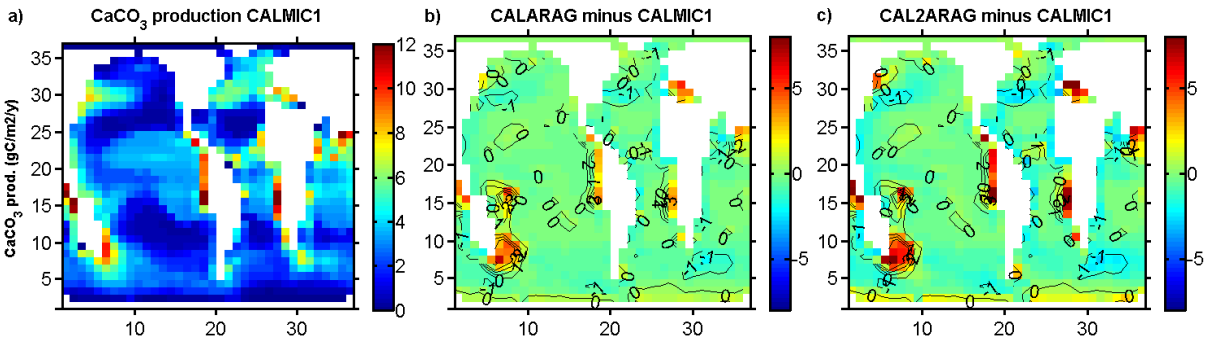

Figure 3. Vertically integrated $CaCO_3$ production for a) the version CALMIC1 that represents calcite production by nanophytoplankton only, b) the difference to version CALARAG that represents calcite and aragonite production and c) the difference to CAL2ARAG that represents calcite production by nano- and mesozooplankton and aragonite production.

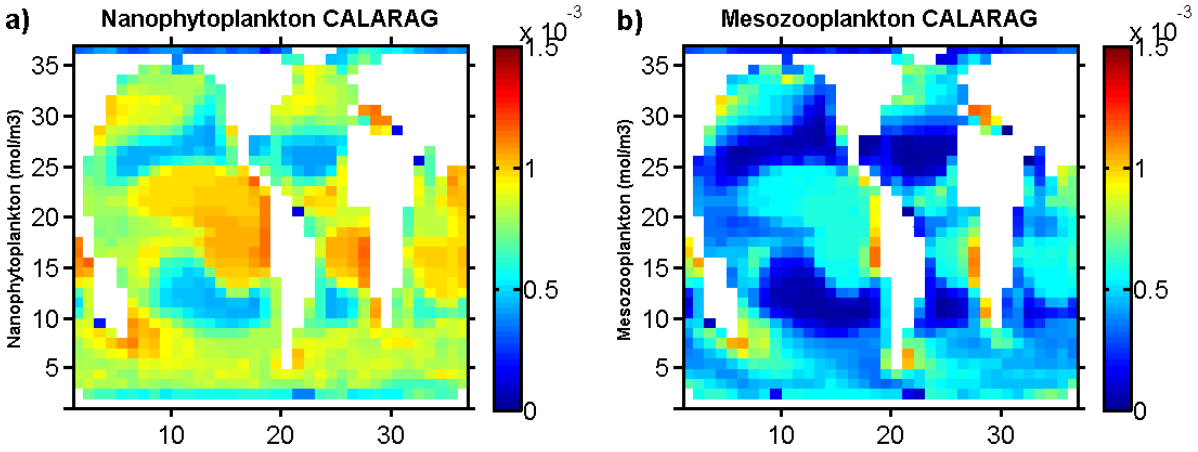

Figure 4. Spatial distribution of a) nanophytoplankton and b) mesozooplankton concentration of the CALARAG model version.

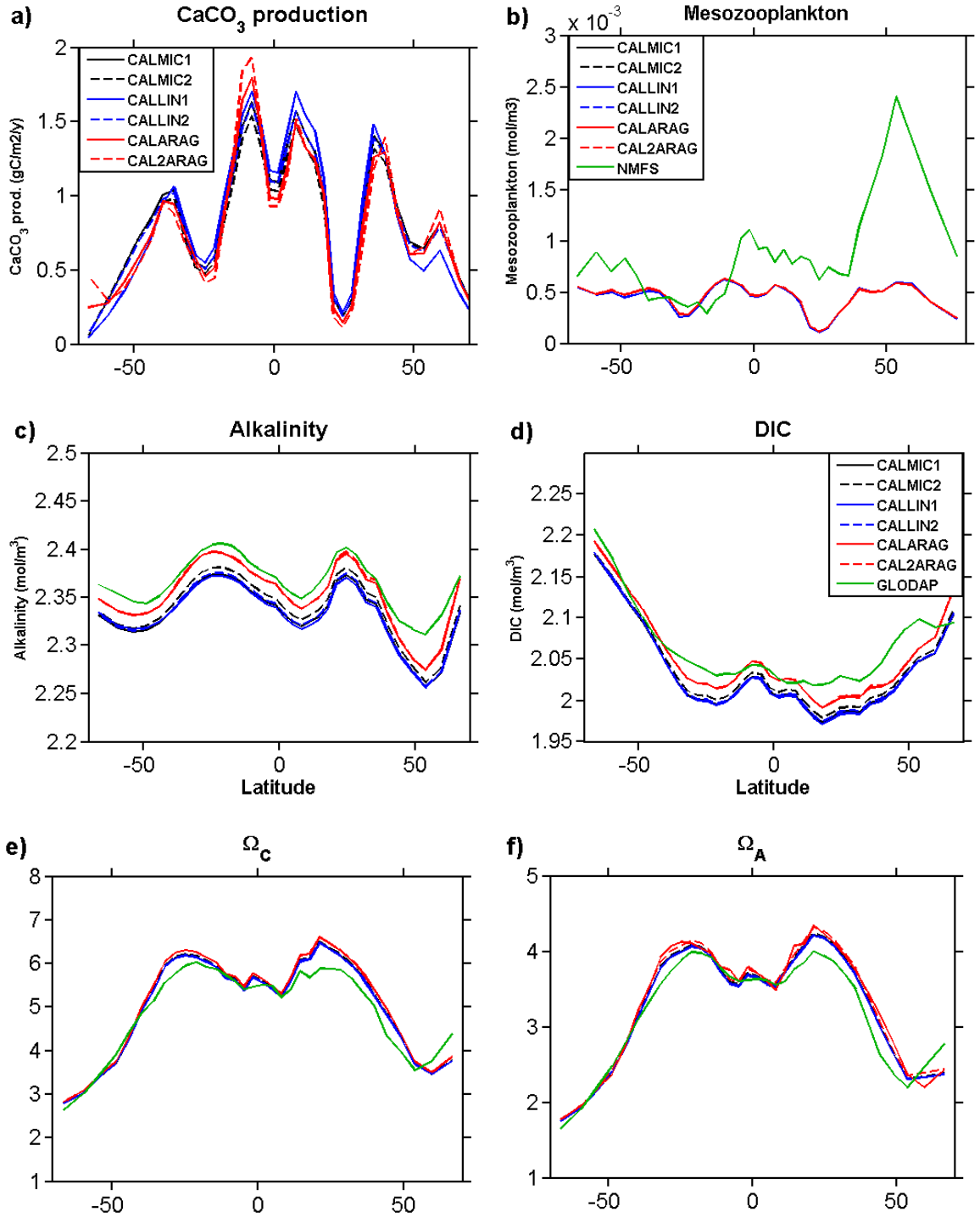

Figure 5. Zonally-averaged a) $CaCO_3$ production, b) mesozooplankton concentration, c) alkalinity, d) DIC, e) calcite saturation state and f) aragonite saturation state for the global ocean and different parameterizations of $CaCO_3$ production in the Bern3D/PISCES model. Observations and observation-based estimates are shown by violet (NMFS data set,

Buitenhuis et al., 2006) and green lines (GLODAP; Key et al., 2004). All concentrations are averages over the upper 3 layers of the model, equivalent to a depth of 126 m.

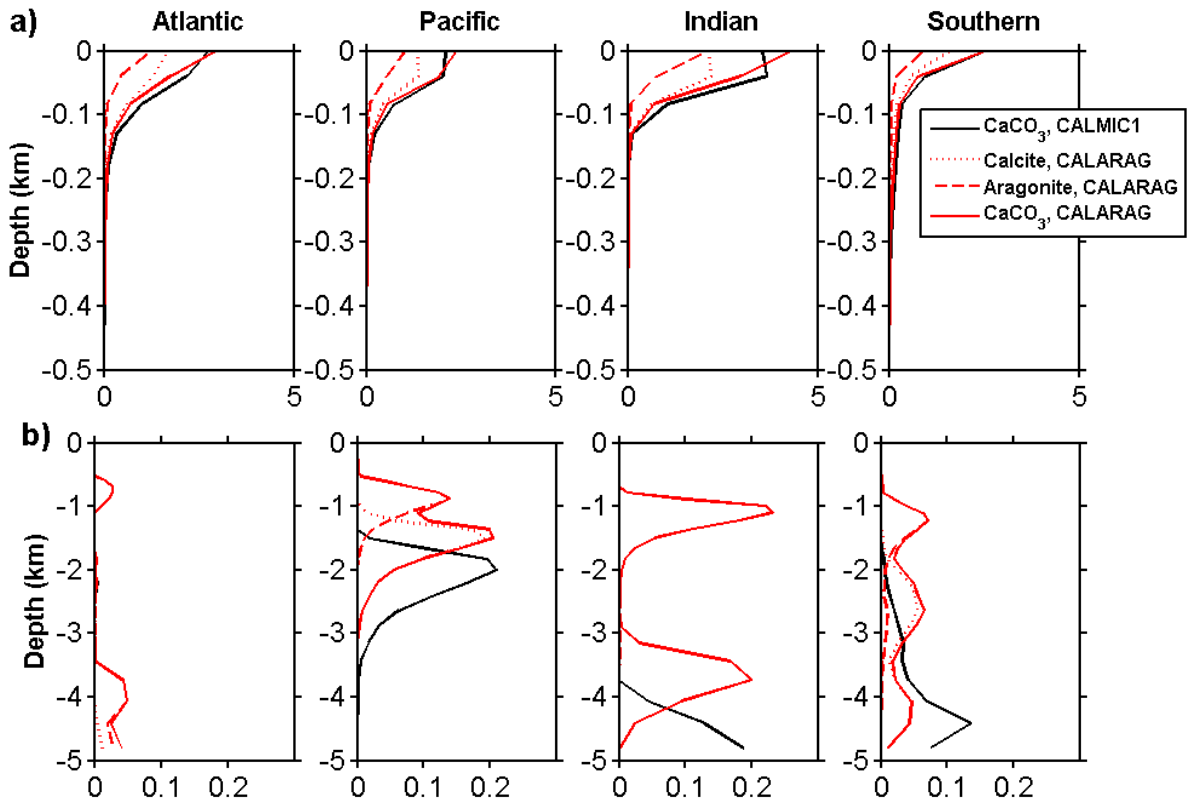

Figure 6. Depth profiles for a) $CaCO_3$ production (µmol $kg^{-1}y^{-1}$) and b) open water $CaCO_3$ dissolution (µmol $kg^{-1}y^{-1}$) of two versions CALMIC1 (calcite, black) and CALARAG (calcite, aragonite and total $CaCO_3$, red). Production of total $CaCO_3$ is shown for the upper 500 m, dissolution for the entire water column.

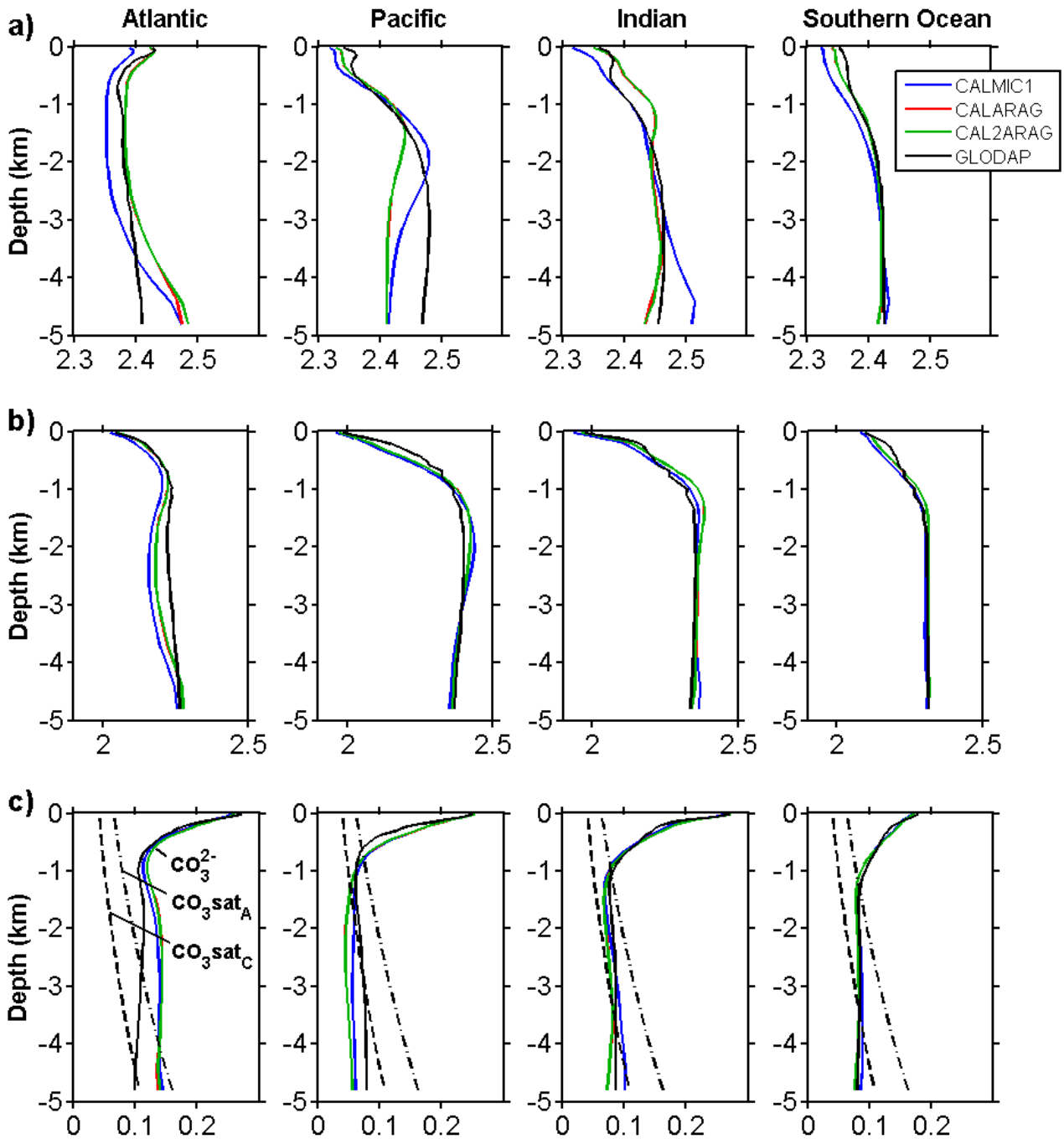

Figure 7. Depth profiles for a) alkalinity (mol m^{-3}), b) DIC (mol m^{-3}), c) CO_3^{2-} (mol m^{-3}), d) $CaCO_3$ production (µmol $kg^{-1}y^{-1}$) and e) open water $CaCO_3$ dissolution (µmol $kg^{-1}y^{-1}$). Concentrations are shown for the Bern3D/PISCES versions CALMIC1, representing calcite production by nanophytoplankton only (blue), CALARAG, representing calcite and aragonite production (red) and CAL2ARAG, representing calcite production by nano- and mesozooplankton and aragonite production (green). Observation-based estimates are shown

by black solid lines (GLODAP; Key et al., 2004) and saturation concentrations for CO_3^{2-} with respect to calcite and aragonite are indicated by black, dashed lines.

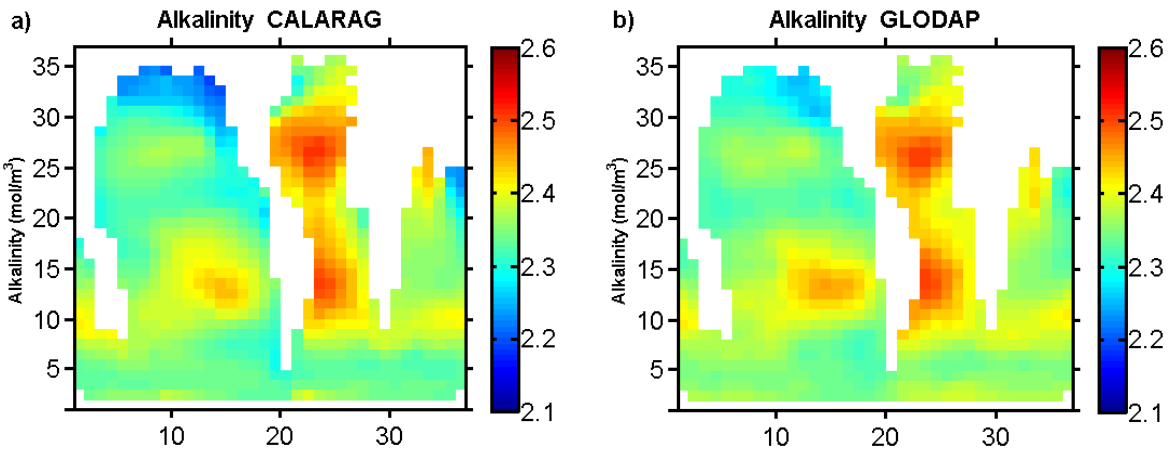

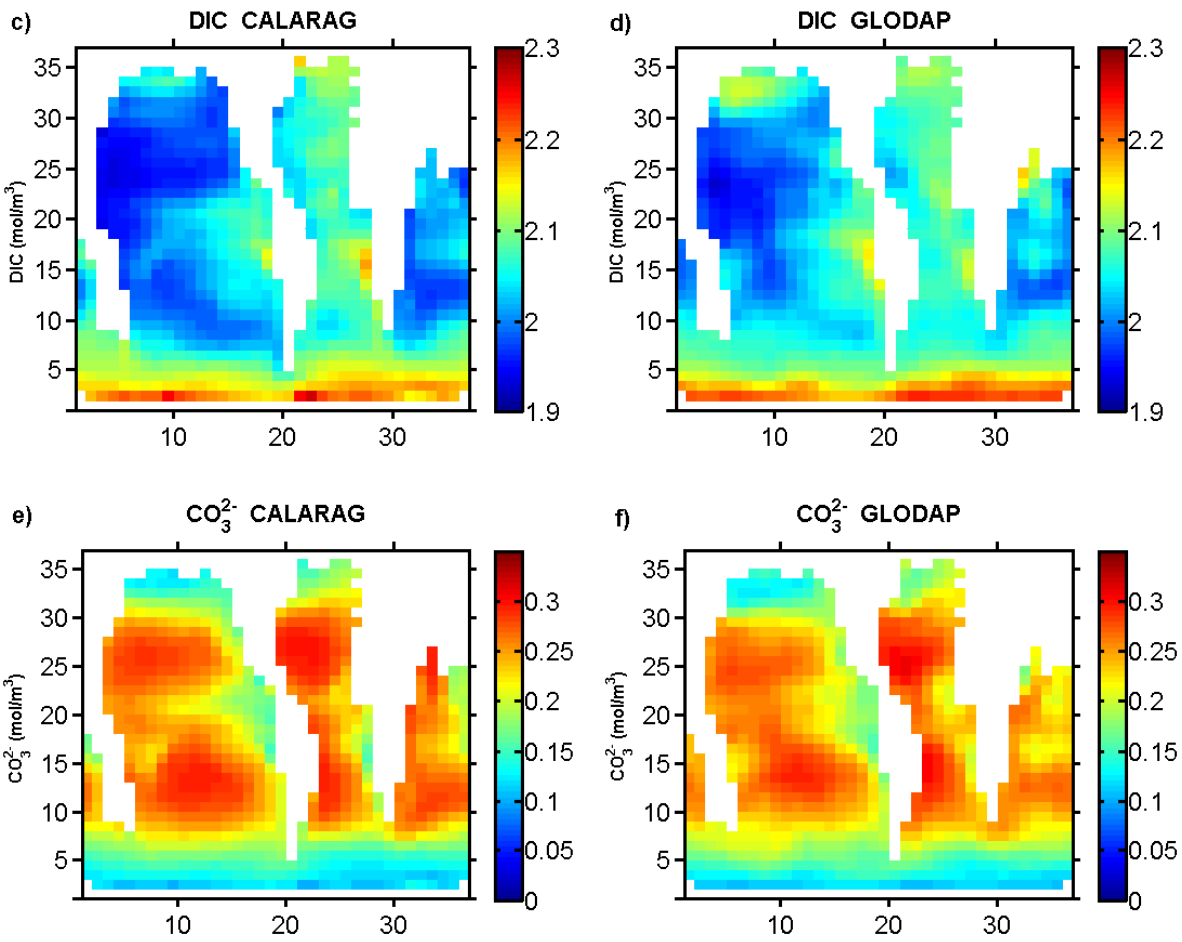

Figure 8. Distribution of (a, b) alkalinity, (c, d) DIC and (e, f) carbonate ion concentrations simulated by the Bern3D/PISCES model (left) and from the GLODAP data (right; Key et al., 2004). Values are from the model version CALARAG that represents calcite and aragonite production and shown are averages over the top 3 layers of the model, equivalent to a depth of 126 m.

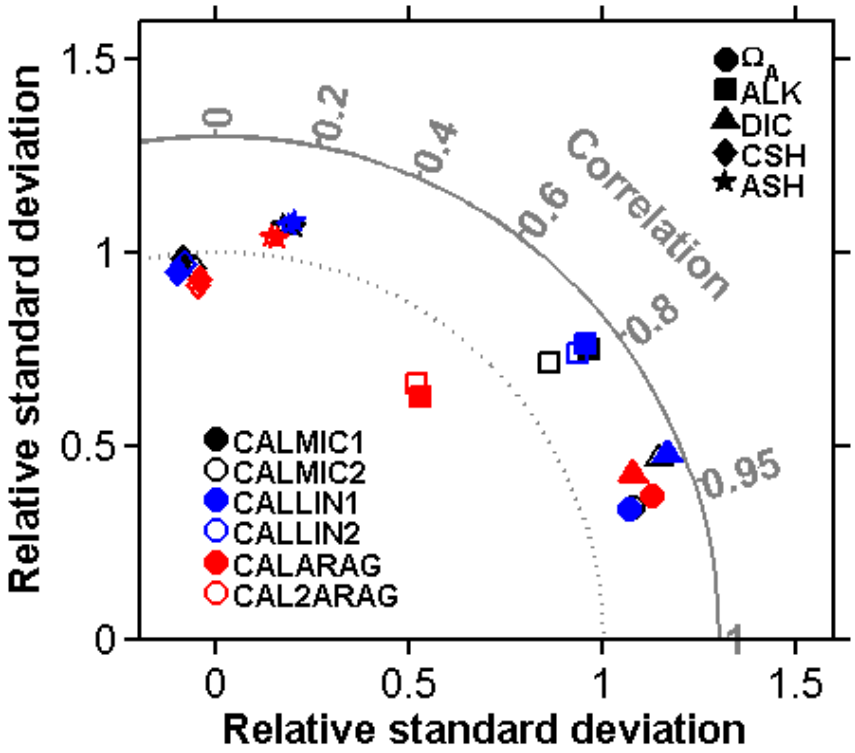

Figure 9. Taylor diagram comparing modeled global fields of aragonite saturation state, alkalinity, and DIC for different parameterizations of the $CaCO_3$ production to observation-based estimates (GLODAP; Key et al., 2004). The modeled and estimated saturation horizons with respect to calcite (CSH) and aragonite (ASH) are added.

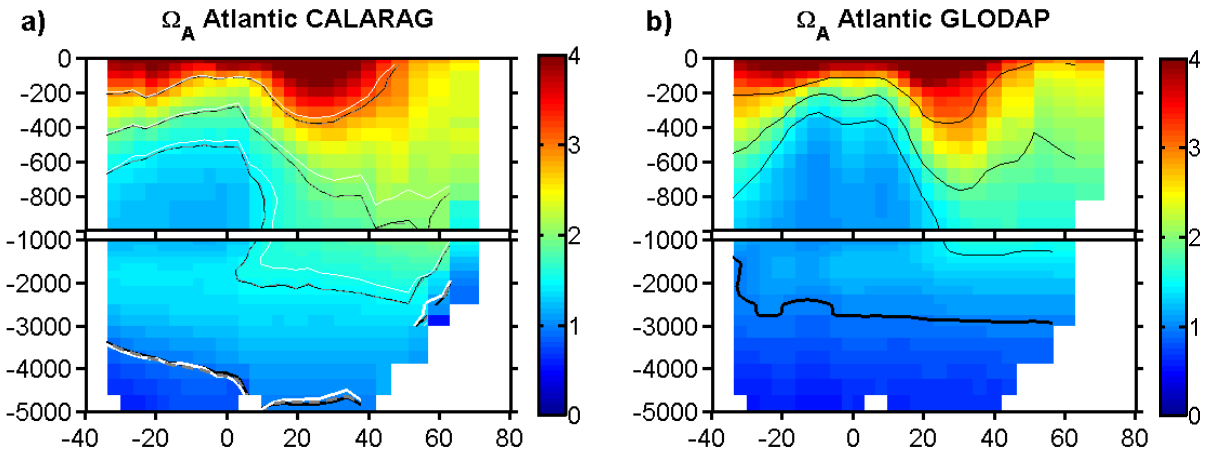

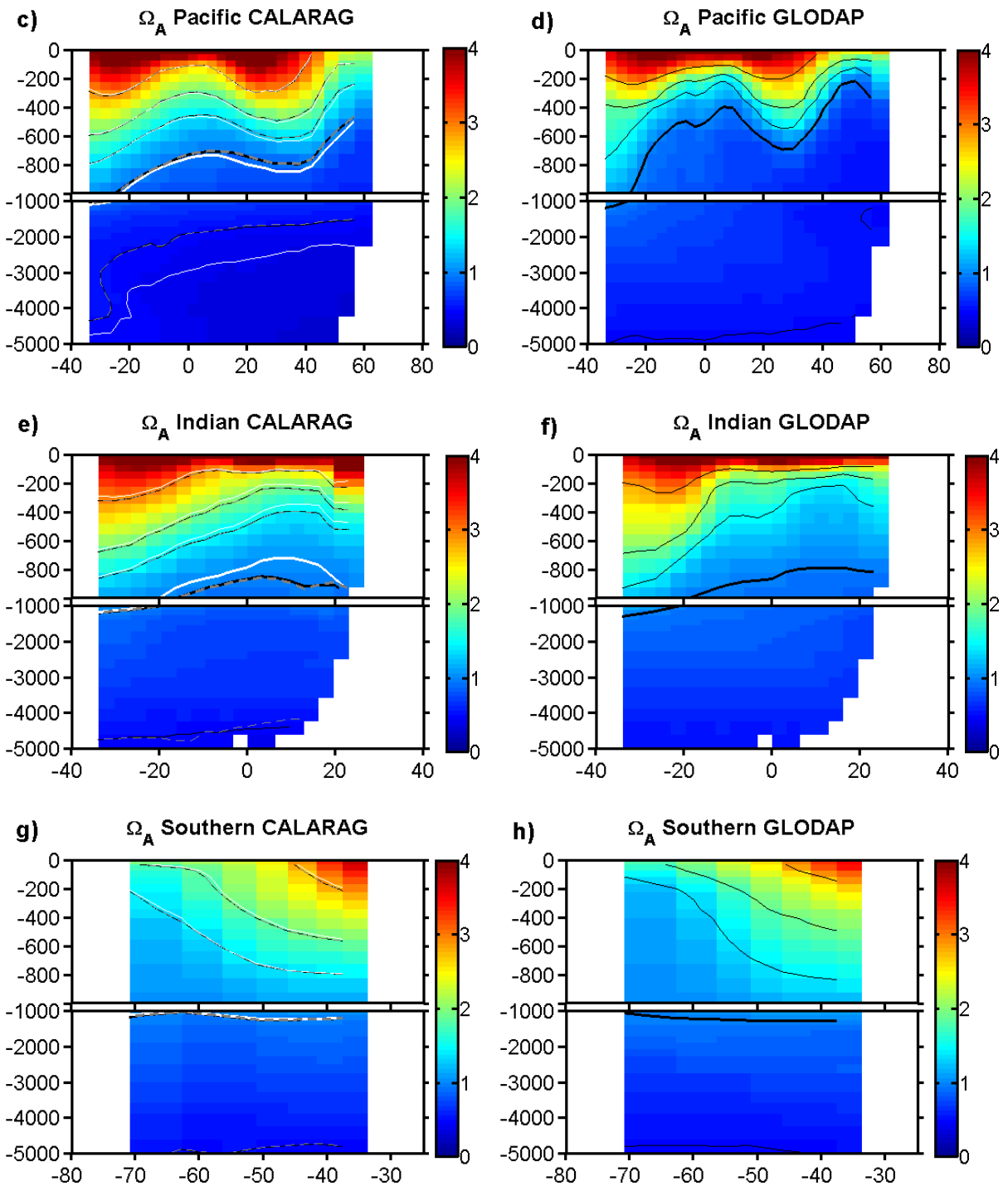

Figure 10. Distribution of the aragonite saturation state simulated by the Bern3D/PISCES model (left; version CALMIC1) and based on observations from GLODAP (right). The saturation horizon in a), c), e) and g) is given for the $CaCO_3$ production parameterizations CALMIC1 (white, calcite only), CALARAG (black, calcite and aragonite production) and CAL2ARAG (grey, calcite by both nano- and mesozooplankton and aragonite). Values represent zonal averages.

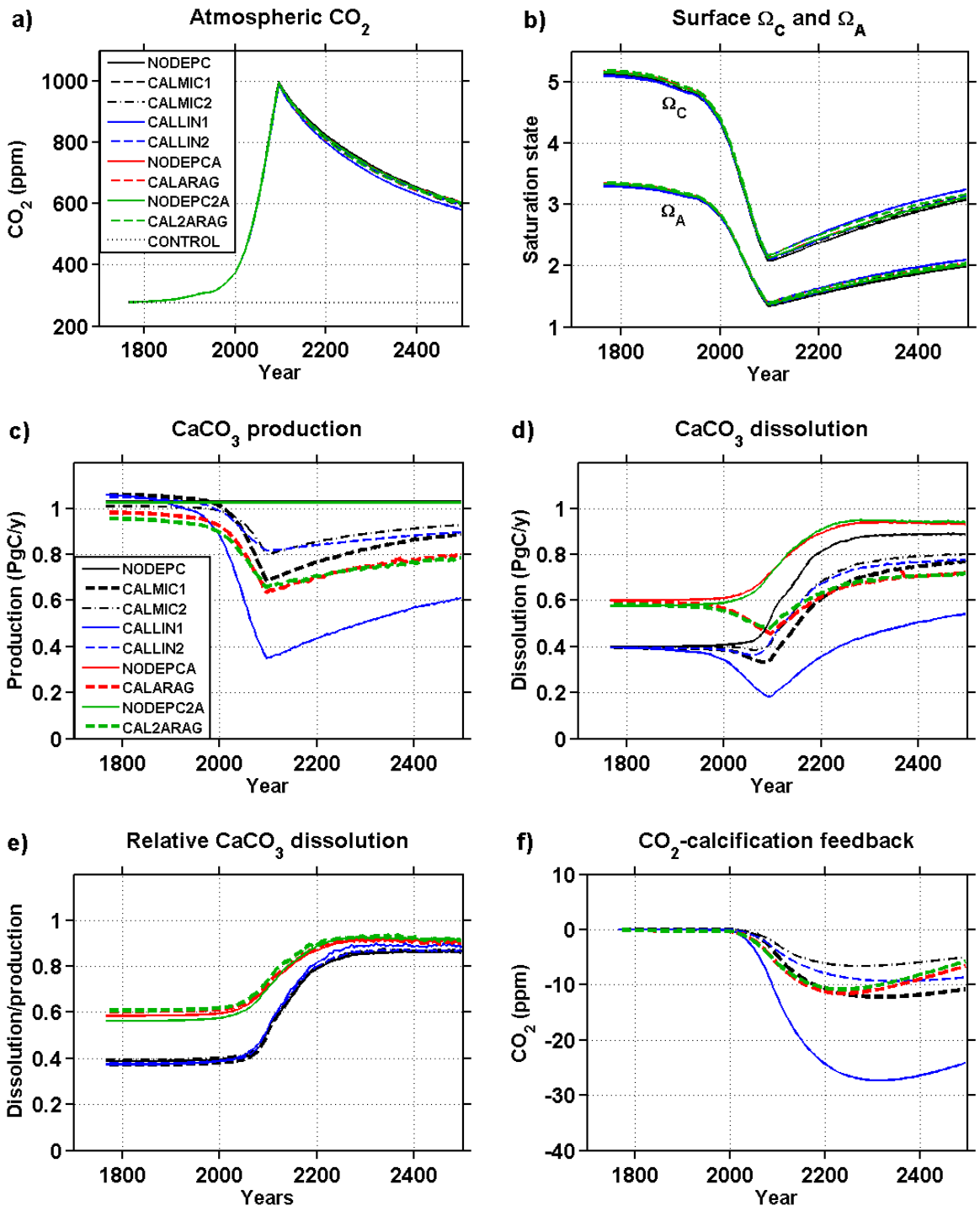

Figure 11. Influence of different $CaCO_3$ production parameterizations for projected a) atmospheric CO_2, b) global-mean surface saturation states with respect to calcite and aragonite, c) global $CaCO_3$ production, d) global, open water $CaCO_3$ dissolution, e) global relative dissolution, and f) the CO_2 – $CaCO_3$ production/dissolution feedback quantified as the difference in atmospheric CO_2 between simulations with and without a dependency of $CaCO_3$ production on the saturation state. The Bern3D/PISCES model was forced with 21st carbon

emissions from the high-emission scenario and emissions are hypothetically set to zero after 2100.

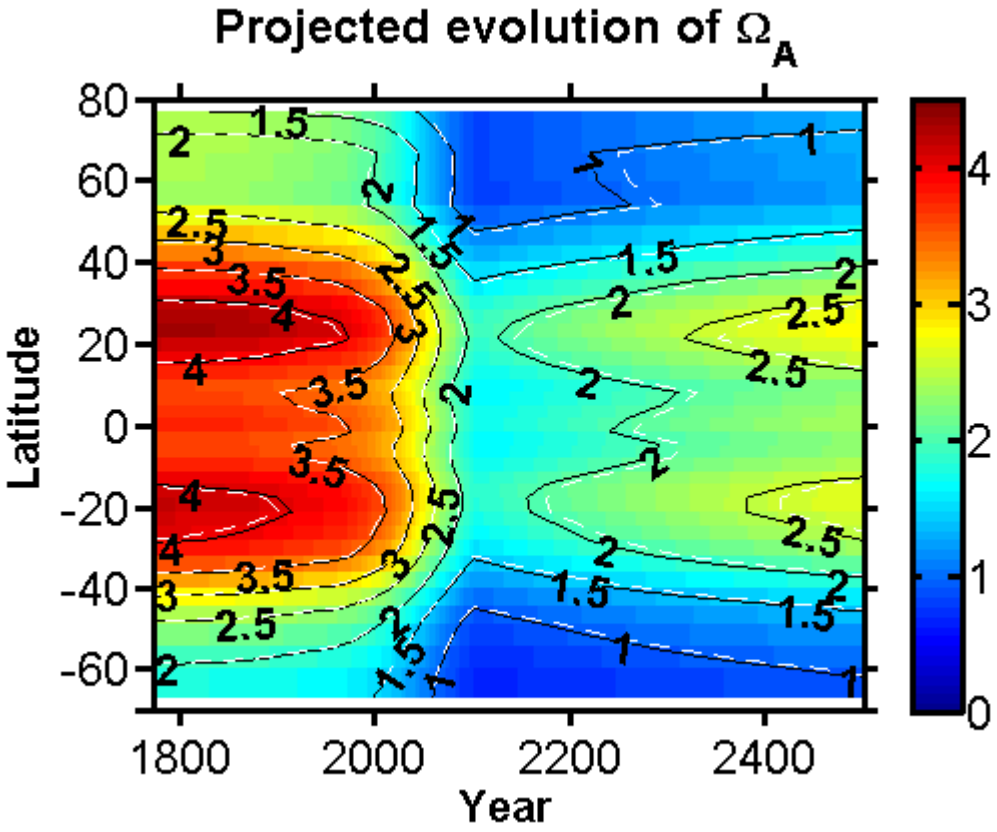

Figure 12. Projected evolution of the aragonite saturation state in the surface ocean (top 125 m) for the High emission commitment scenario where carbon emissions increase in the 21st century following scenario RCP8.5. Color scale and black contour lines represent values from the CALARAG version that includes aragonite and calcite production. White contour lines are from the version with $CaCO_3$ production independent of the saturation state (NODEPCA).

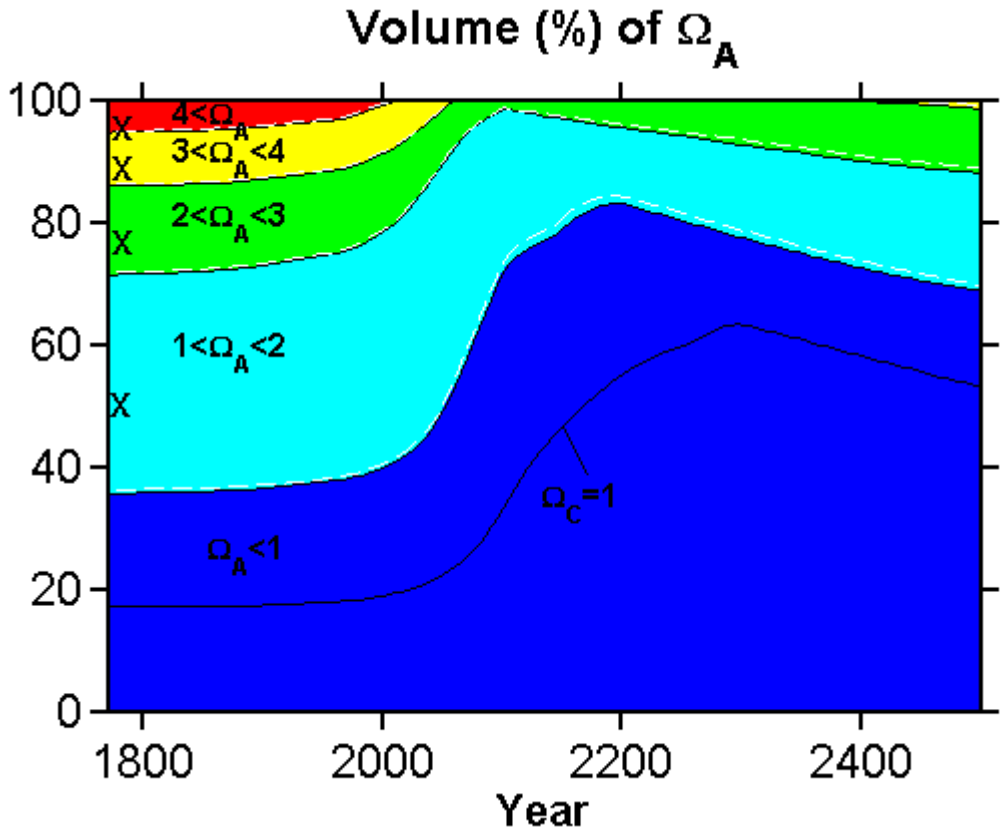

Figure 13. Simulated global annual mean changes in the entire ocean volume of supersaturated (light blue to red) and undersaturated (blue) waters with respect to aragonite for the High emission commitment scenario where emissions are set to zero after 2100. Differences are small between the versions with (color, black contours), and without (white contours) $CaCO_3$ production depending on saturation. The black dashed line indicates the separation between over and undersaturated water with respect to calcite. The crosses denote the respective volumes of pre-industrial saturation state derived from the GLODAP data set.

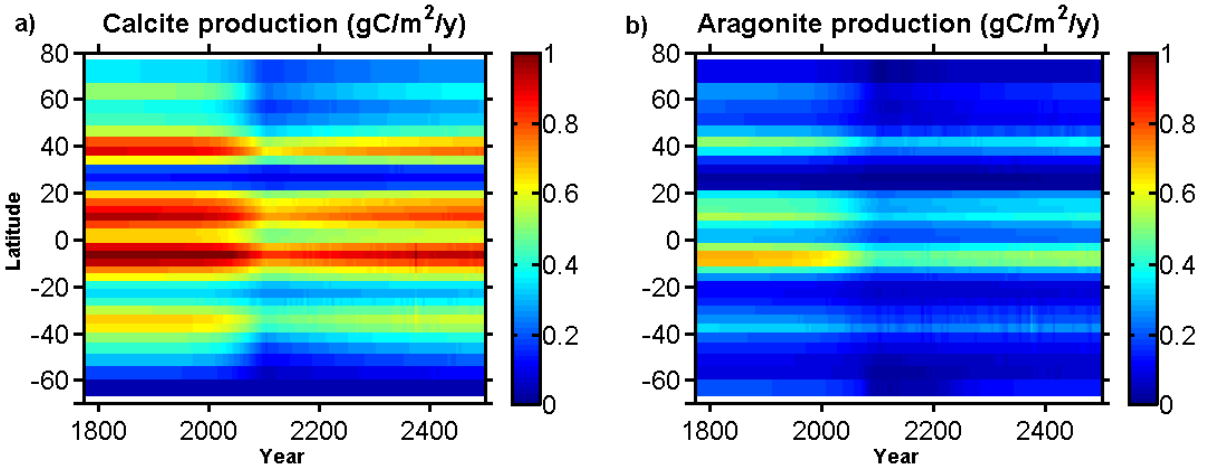

Figure 14. Projected evolution of a) calcite and b) aragonite production (g C m^{-2} y^{-1}) for the CALARAG version.

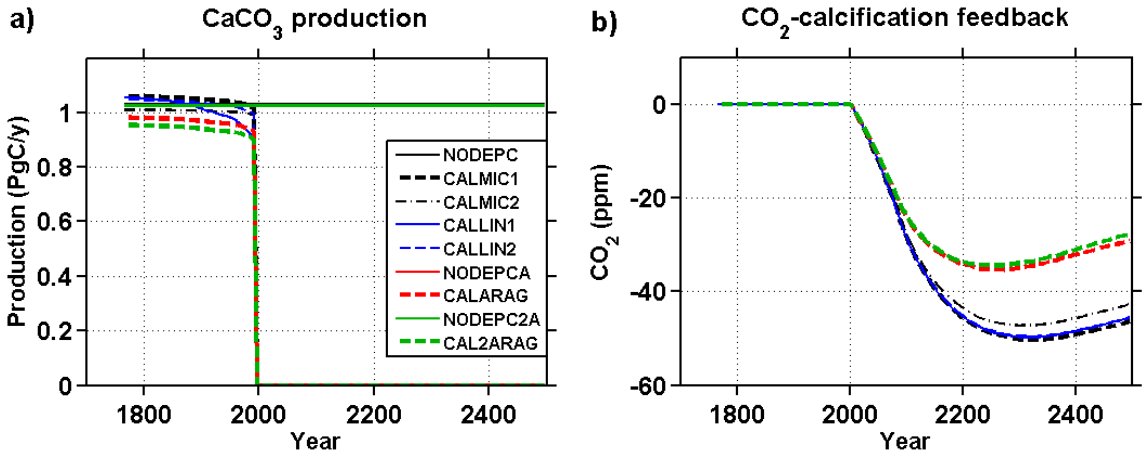

Figure 15. Sensitivity of the different $CaCO_3$ production parameterizations to setting the global $CaCO_3$ production to 0 after the year 2000, as shown in a). Subfigure b) illustrates the subsequent maximum potential value of the CO_2 – $CaCO_3$ production/dissolution feedback.

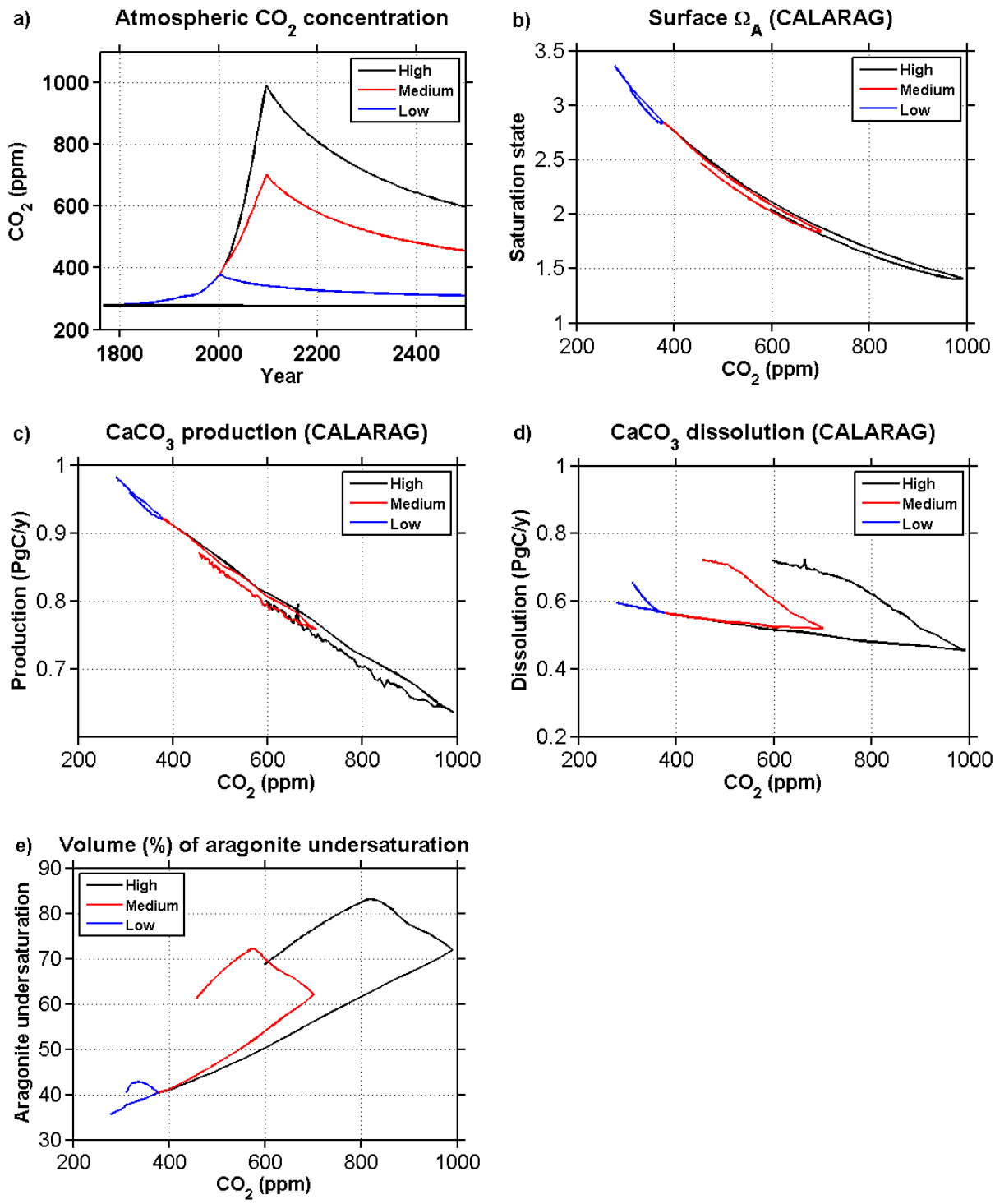

Figure 16. Projected global mean values for a High, Medium, and Low emission scenario and for the Bern3D/PISCES version that includes aragonite and calcite production (CALARAG). Evolution of a) atmospheric CO_2 as a function of time, b) aragonite saturation state, c) total $CaCO_3$ production, d) open water $CaCO_3$ dissolution and e) volume of aragonite undersaturation are shown as functions of atmospheric CO_2.

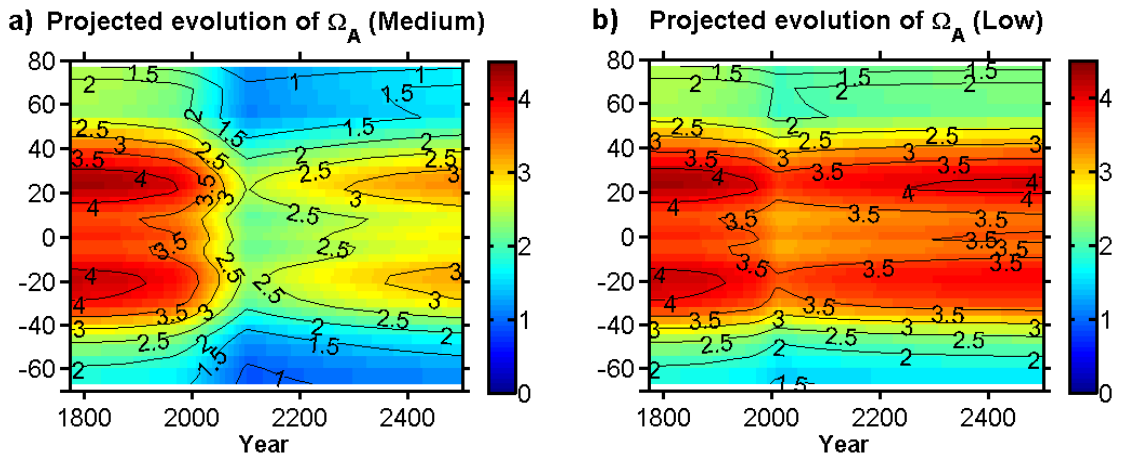

Figure 17. Modeled evolution of zonal annual mean surface aragonite saturation state of the a) Medium and b) Low emission commitment scenario and the CALARAG model version.